

El Niño variability in simple ocean data assimilation (SODA), 1871–2008

Benjamin S. Giese¹ and Sulagna Ray¹

Received 30 September 2010; revised 15 November 2010; accepted 3 December 2010; published 17 February 2011.

[1] A new ocean reanalysis that covers the period from 1871 to 2008 is used to explore the time-evolving characteristics of El Niño. The new reanalysis assimilates all available hydrographic and sea surface temperature data into a model of the global ocean forced with surface boundary conditions from an atmospheric reanalysis that also covers the period from 1871 through 2008. Using traditional measures of El Niño, our reanalysis shows that the timing of El Niño events is in agreement with sea surface temperature reconstructions, but El Niño in the reanalysis is stronger, particularly from 1871 to 1920. A new index based on the first moment of the temperature anomaly is introduced. The new index is used to characterize the strength and location of El Niño events and has the advantage that it is independent of the location of El Niño. Using the new index, El Niño in the reanalysis shows prominent decadal variability of strength but relatively little long-term trend. El Niño events were strong in the last part of the 19th century and first part of the 20th century and again in the latter part of the 20th century, with weak El Niño events in the middle of the 20th century. The location of El Niño also varies considerably, ranging from the western to the eastern Pacific near the coast of South America. However, the null hypothesis that the location of El Niño can be represented as a random distribution about a central longitude of about 140°W cannot be rejected.

Citation: Giese, B. S., and S. Ray (2011), El Niño variability in simple ocean data assimilation (SODA), 1871–2008, *J. Geophys. Res.*, 116, C02024, doi:10.1029/2010JC006695.

1. Introduction

[2] Over the past 2 decades our understanding of the mechanisms that control the structure of El Niño has increased tremendously. There are now comprehensive theories that describe the timing, the duration, and the seasonality of El Niño events [Cane and Zebiak, 1985; Schneider et al., 1995; Goddard and Philander, 2000; Meinen and McPhaden, 2000; Cane, 2005]. Despite this comprehensive analysis of what might arguably be the most studied mode of climate variability, there is far less understanding of its long-term variations. Since El Niño brings about worldwide consequences such as suppressed summer monsoon precipitation over the Indian peninsula and parts of Australia [Rasmusson and Carpenter, 1983; Ropelewski and Halpert, 1987; Power et al., 1999], precipitation anomalies across North America [Ropelewski and Halpert, 1986], and decreased North Atlantic tropical cyclone and hurricane activity [Pielke and Landsea, 1999; Fedorov et al., 2010], it is clearly important to document and describe changes in El Niño.

[3] There are numerous published articles that describe trends and decadal variations in El Niño. These variations

include changes in El Niño frequency [Trenberth and Hoar, 1996; An and Wang, 2000], El Niño strength [Zhang et al., 2008; Vecchi and Wittenberg, 2010], and the location of warming during El Niño [Yeh et al., 2009].

[4] Several studies document a change in the frequency of El Niño, most prominently in the last few decades [An and Wang, 2000; Trenberth and Hoar, 1996]. Mitchell and Wallace [1996], An and Wang [2000], and Fedorov and Philander [2000] show a weakening of easterlies west of the dateline and a change in the periodicity of El Niño from about 3 years to about 5 years coincident with a deepening of the thermocline [Fedorov and Philander 2000] from the 1960s to the 1990s.

[5] In addition to evidence of the changing frequency of El Niño, recent papers have also proposed that El Niño has strengthened in recent years [Gu and Philander, 1995; Trenberth and Hoar, 1996, 1997; Vecchi and Wittenberg, 2010]. These changes are sometimes described as resulting from (or contributing to) decadal variability. Other studies characterize the change in strength as a trend, possibly related to global warming [Trenberth and Hoar, 1996; Timmermann et al., 1999; Fedorov and Philander, 2000; Vecchi et al., 2006; Power and Smith, 2007].

[6] The cause for increased frequency or increased strength of El Niño has often been ascribed to changes in the mean state of the Pacific Ocean associated with a weakening of tropical Pacific atmospheric circulation [Wang and An, 2001; Vecchi et al., 2006], possibly in response to global

¹Department of Oceanography, Texas A&M University, College Station, Texas, USA.

warming [Power and Smith, 2007; Ye and Hsieh, 2008; Yang and Zhang, 2008; Vecchi et al., 2008; Collins et al., 2010]. A change in the mean state of wind and thermocline depth can determine which dynamical state the evolution El Niño would follow. Fedorov and Philander [2000] and Philander and Fedorov [2003] show that a deep thermocline with strong winds in the east favors the delayed oscillator mode in which the sea surface temperature variations occur in response to the vertical movement of the thermocline. A shallow thermocline favors a local mode in which the SST (sea surface temperature) variation is affected by cold water entrained across the thermocline.

[7] The cause of such decadal changes could be complex, involving a wide range of timescales. For example a change of anomalous westerlies in the western equatorial Pacific at the onset phase of an El Niño might induce changes in the timing of the coastal warming off the South American coast [Wang, 1995]. Recent studies emphasize the importance of tropical Pacific Ocean circulation and, in particular, the role of subtropical cells, as a mechanism linking wind stress variations and tropical Pacific SST [Nonaka et al., 2002; Capotondi et al., 2005]. In addition to changes in the tropical Pacific, remote forcing, such as midlatitude changes [Kleeman et al., 1999] and weakening of the Atlantic thermohaline circulation [Timmermann et al., 2005], have also been cited to be possible reasons for decadal changes in El Niño–Southern Oscillation (ENSO).

[8] There have also been recent studies that suggest that the location of El Niño warming has changed in recent years. For example, Wang [1995] notes a decadal change in wind anomalies and position of the SST anomaly at the onset of El Niño. Since the location of El Niño warming can have a profound effect on teleconnection patterns such as failure of the Indian monsoon [Kumar et al., 2006] and in the temperature and precipitation over the United States [Ashok et al., 2007; Kim et al., 2009], change in the structure of El Niño has the potential to have a profound impact on Earth's climate.

[9] Recent studies suggest that it is not just that the location of El Niño varies but that there are, in fact, different kinds of El Niño [Wang, 1995; Trenberth and Stepaniak, 2001; Larkin and Harrison 2005; Ashok et al., 2007; Kao and Yu, 2009; Kug et al., 2009]. Although the names and definitions of these El Niño types are slightly different, they all describe a central Pacific El Niño in which the warmest SST anomaly occurs in the western central Pacific, and an eastern Pacific type, the canonical El Niño type in which the warmest SST anomaly extends away from the South American coast to the central Pacific. Larkin and Harrison [2005] calls it a dateline El Niño, whereas Ashok et al. [2007] call the central and western Pacific warming El Niño Modoki, Kao and Yu [2009] name the anomalous warming pattern the central Pacific–El Niño, and Kug et al. [2009] call it a warm pool El Niño. However, these studies rely on records of El Niño that are relatively short. The Ashok et al. study covers the period from 1979 to 2005, Kao and Yu look at the period from 1950 to 2001, and Kug et al. consider the period from 1970 to 2005. The longest of these records, from 1950 to 2001, includes just 7 conventional El Niño and 17 nonconventional El Niño events as defined by Kao and Yu [2009]. In a recent study, Lee and McPhaden [2010] use a record of El Niño from 1982 through 2009 to

suggest that the central Pacific type of El Niño is increasing in strength. Since El Niño occurs at intervals of about 4 years, all of these studies are based on relatively few members.

[10] Our ability to document and describe the change of El Niño is severely hampered by a lack of observations in the tropical Pacific Ocean before the 1950s. This lack of observations makes it difficult to differentiate between trends and long-term variability given the short length of data records for much of the oceans. This problem is particularly acute in the tropical and Southern Hemisphere oceans for which comprehensive ocean temperature observations exist at best only in the second half of the 20th century. As a result of limited observations, scientists often rely on sea surface temperature (SST) reconstructions [Kaplan et al., 1998; Rayner et al., 2003], which combine temporal records of SST at a few locations with typical spatial patterns of SST observed in later decades of more abundant data. A limitation of this methodology is that it assumes that the spatial patterns of SST variability do not change over time.

[11] An alternative method is to use an ocean model in conjunction with data assimilation to estimate the state of the oceans. Data assimilation schemes have been developed to optimally merge sparse observational data sets with state-of-the-art ocean models to provide an estimation of the time-evolving state of the oceans. One such assimilation product is simple ocean data assimilation (SODA), which has been developed to study ocean climate variability on time scales that range from seasons to decades over the period from 1958 to 2007 [Carton et al., 2000a, 2000b; Carton and Giese, 2008]. These studies, particularly for decadal time scales, are hampered by the relatively short duration of the reanalysis.

[12] Until recently, it was not possible to model the state of the tropical Pacific Ocean before the 1950s, primarily because of the lack of surface meteorological forcing data. However, a new reanalysis data set (designated 20CRv2 [Whitaker et al., 2004; Compo et al., 2006]) of the atmospheric circulation for the period 1871 through 2008 provides us with this missing atmospheric forcing data set and allows us to model the ocean state starting at the beginning of the 20th century. We use the 20CRv2 atmospheric reanalysis data set to force the SODA global ocean model. The result is an oceanic reanalysis for the period from 1871 to 2008. In this paper we use this new ocean reanalysis to describe the evolving nature of El Niño.

2. Methods

2.1. Simple Ocean Data Assimilation

[13] For this study we use the SODA methodology [Carton and Giese, 2008], including the Parallel Ocean Program (POP) ocean model and the SODA software. Two experiments were carried out for this study; SODA 2.2.4, which uses data assimilation, and SODA 2.2.0, identical to the first except without data assimilation. The ocean model is based on POP version 2.0.1 numerics [Smith et al., 1992] with a horizontal resolution that is on average $0.4^\circ \times 0.25^\circ$ and with 40 levels in the vertical. The grid is distorted in northern latitudes to allow for a displaced North Pole (in order to resolve the Arctic Ocean) and meridional resolution increases in the poleward direction to reduce the grid anisotropy that comes about in Mercator coordinate grids

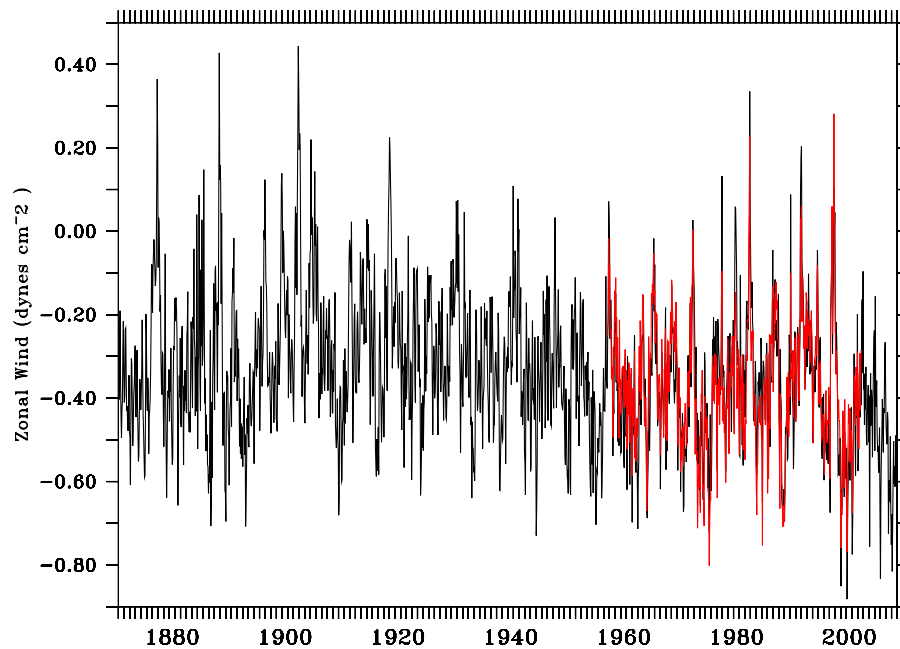


Figure 1. Zonal wind stress in dyn cm^{-2} in the Niño 4 (160°E – 150°W and 5°S – 5°N) region for the 20CRv2 (black line) and for ERA-40 (red line).

due to the convergence of meridians at high latitudes. Vertical mixing uses the K-profile parameterization, while horizontal mixing is biharmonic. Rivers are included with climatological seasonal discharge. There is no explicit sea ice model although surface heat flux is modified when the surface temperature reaches the freezing point of seawater. This model has been used in past versions of the SODA ocean reanalysis [Carton *et al.*, 2000a, 2000b; Carton and Giese, 2008].

[14] The assimilation is carried out sequentially using a 10 day update cycle with model error covariances determined from a simulation that does not include assimilation. The error covariances evolve in time as a function of the local velocity field and mixed layer depth. Updating is done incrementally following Bloom *et al.* [1996] to suppress excitation of spurious variability. Output variables are averaged every 5 days, and are then mapped onto a uniform global $0.5^{\circ} \times 0.5^{\circ}$ horizontal grid using the horizontal grid spherical coordinate remapping and interpolation package of Jones [1999].

[15] The ocean model surface boundary conditions are provided from a new atmospheric data set [Whitaker *et al.*, 2004; Compo *et al.*, 2006, 2008] designated as 20CRv2. The surface wind stress from 20CRv2 is used in the ocean model for the surface momentum fluxes. Solar radiation, specific humidity, cloud cover, 2 m air temperature, precipitation and 10 m wind speed from 20CRv2 are used for computing heat and freshwater fluxes.

[16] The atmospheric reanalysis includes only surface observations of synoptic pressure and monthly SST and sea ice distribution from the HadISST 1.1 data set [Rayner *et al.*, 2003]. The atmosphere reanalysis uses a state-of-the-art data assimilation methodology called the ensemble filter described by Whitaker and Hamill [2002]. This reanalysis relies on a model similar to that used in the original National Center for Environmental Prediction/

National Center for Atmospheric Research (NCEP/NCAR) reanalysis with a 192×94 horizontal Gaussian grid [Kalnay *et al.*, 1996]. Differences between the construction of this new reanalysis and the NCEP/NCAR reanalysis include limiting the observation set to only sea level pressure observations and SST, and use of an upgraded ensemble Kalman filter data assimilation algorithm. The limited observation set is used to reduce the appearance of spurious climate signals created by changes in the observing system which has limited the use of the NCEP/NCAR reanalysis for studies of decadal variability [Sturaro, 2003; Pohlmann and Greatbatch, 2006].

[17] We are particularly interested in ENSO, and so we begin by comparing the 20CRv2 surface wind stress with wind stress from ERA-40 [Uppala *et al.*, 2005] that has been used in prior SODA reanalyses [Carton and Giese, 2008]. Monthly mean zonal wind stress in the Niño 4 region (160°E to 150°W and 5°S to 5°N) is shown for 20CRv2 and ERA-40 in Figure 1. For the period for which they overlap the two wind products agree very well in the Niño 4 region. Both capture the large ENSO events of 1982/1983 and 1997/1998, and both contain what looks like lower frequency variability. The two products are highly correlated ($r = 0.86$) in the period for 1958–2001, during which they overlap. Both wind products also have a trend, with the zonal wind in the Niño 4 region getting progressively stronger. This trend is not only apparent when both products are present (1958–2005), but is also apparent in the first half of the 20th century in the 20CRv2 winds. In the first part of the record, from 1871 to about 1900, there is a slight weakening of the easterly trade winds.

2.2. Data

[18] The temperature and salinity profile data we use have been obtained from the recent release of the World Ocean Database 2009 (WOD09) [Boyer *et al.*, 2009], which is

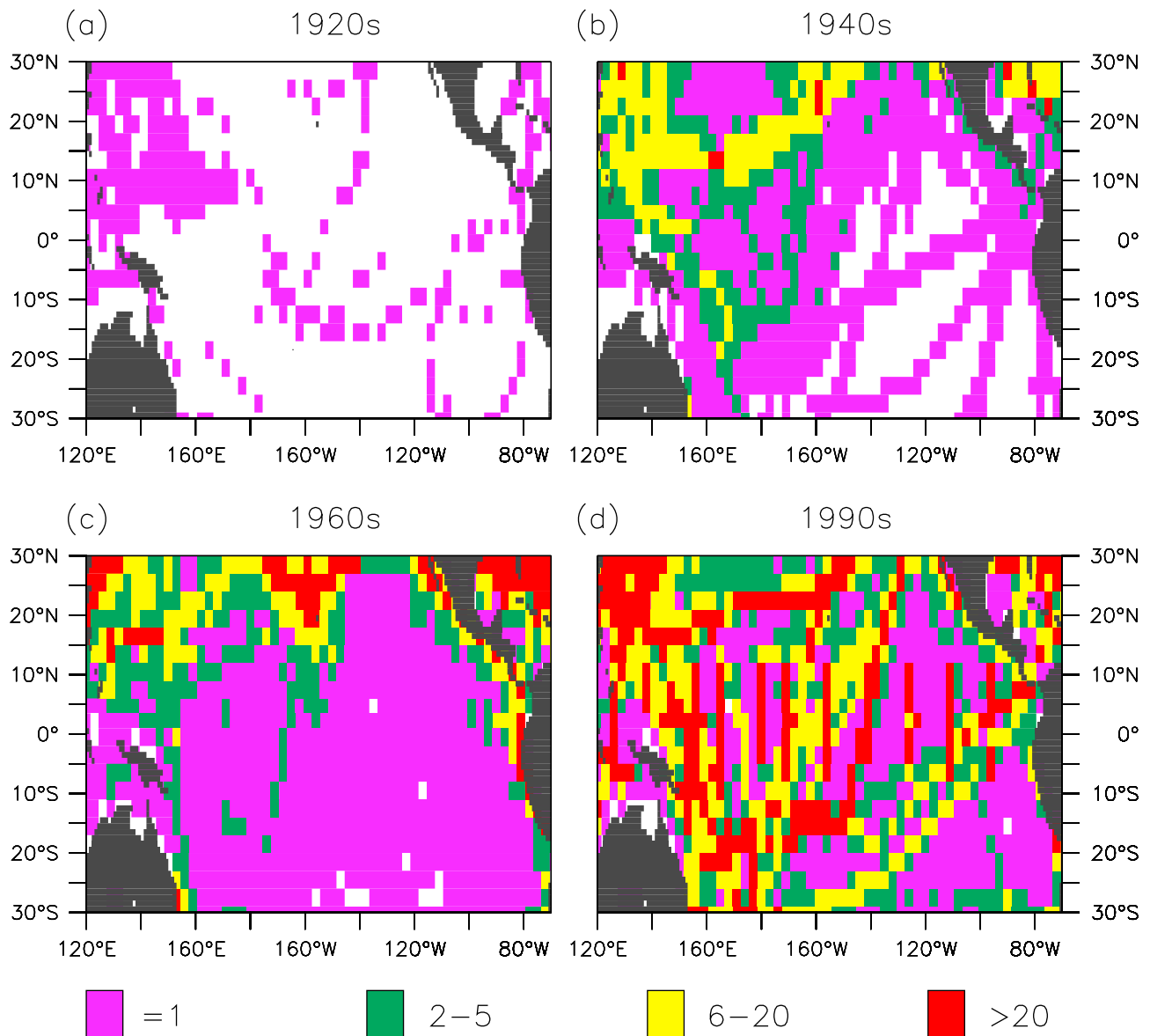


Figure 2. The number of WOD09 hydrographic temperature observations used in SODA 2.2.4 by decade.

substantially updated from previous versions. Using the standard level data means that the expendable bathythermograph (XBT) and mechanical bathythermograph (MBT) observations used in SODA have been corrected for the fall rate error as described by *Levitus et al.* [2009]. The impact of this bias correction on an ocean reanalysis system is described by *Giese et al.* [2011] and has a significant effect on reducing decadal variability, particularly in the North Pacific Ocean. Here we review the spatial and temporal distribution of these data because these factors have a strong influence on what we may expect from a data assimilation-based reanalysis.

[19] In the decade 1900–1909 the majority of the roughly 8000 temperature/salinity profiles available in WOD09 were collected using instruments such as reversing thermometers and bottles, and are confined to the North Atlantic and adjacent Norwegian Sea. Of these, three fourths have depths

shallower than 200 m, and only a relative handful reach 1000 m. By the decade 1920–1929 the observing system had expanded significantly throughout the Atlantic due to data collected during the *Meteor* expeditions [*Defant, 1981*] (see *Arbic and Owens* [2001] for comparisons to later sections) and had begun to expand in the western North Pacific although there are few measurements in the tropical Pacific Ocean (see Figure 2a).

[20] In the 1930s the number of profiles in the western North Pacific continued to grow. The corresponding set of SST measurements is most extensive along ship routes in the northern oceans and, interestingly, across the northern Indian Ocean.

[21] In the late 1930s and 1940s (Figure 2b), use of the MBT leads to a gradual increase in coverage throughout the oceans although with much of the additional data at depths shallower than 300 m. In the late 1940s Ocean Weather

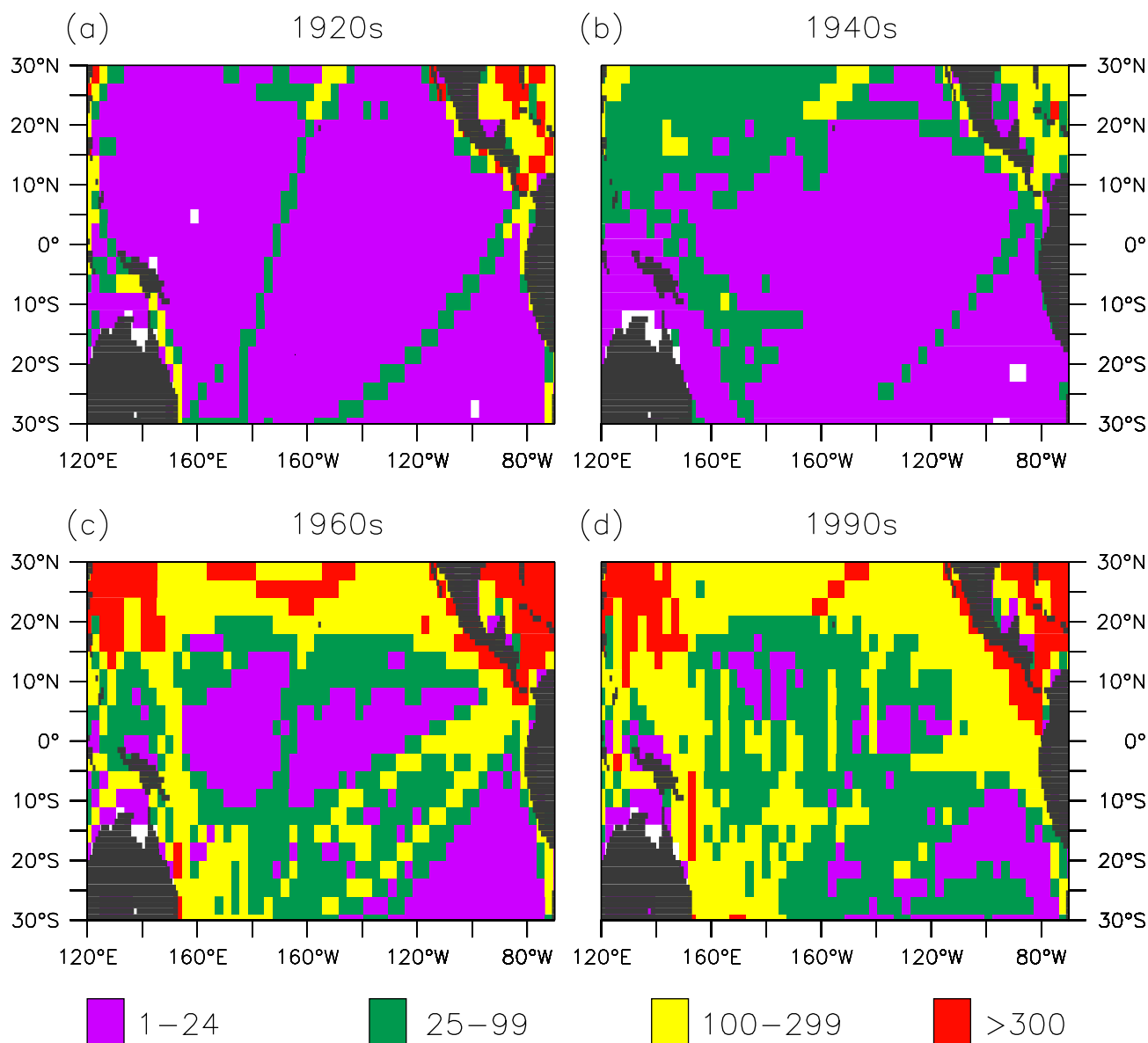


Figure 3. The number of ICOADS 2.5 SST observations used in SODA 2.2.4 by decade.

Station time series were set up in the North Atlantic and Pacific oceans [e.g., *Østerhus and Gammelsrød, 1999*], while the XBT came into use in the late 1960s. This instrument is more convenient to launch than the MBT and reaches greater depth (typically 450 or 780 m) but is known to suffer from bias in the depth estimates [*Hanawa et al., 1995; AchutaRao et al., 2006*].

[22] In recent decades, ocean observing systems have increased dramatically with the expansion of Volunteer Observing Ship XBT routes, the World Ocean Circulation Experiment, deployment of the Tropical Ocean Atmosphere/Triton mooring array and its sister arrays in the Atlantic and Indian oceans, the Global Drifter Program, and the implementation of the Argo profiling system (compare Figure 2d and 2c).

[23] The problem of limited hydrography in the first half of the 20th century is ameliorated to an extent by the use of

SST. For SST observations we use data from ICOADS release 2.5 [*Woodruff et al., 2011*]. The SST data coverage (shown in Figures 3a–3d), particularly in the first half of the 20th century, is considerably greater and covers a greater portion of the globe than the hydrographic data. In addition to assimilating temperature and salinity profile data we have analyzed the WOD09 data combined with ICOADS in situ SST to extract mixed layer properties such as temperature, depth and barrier layer distribution. Data are assimilated into the mixed layer using a method (described by *Carton et al. [2008]*) that helps the model maintain mixed layer properties (mixed layer depth, distribution of barrier layers, etc.). SODA employs a mixed layer formulation in the assimilation of SST, so that in regions of deep mixed layer the surface information extends deeper into the ocean. This has an important impact on quantities such as heat content and sea level height, for which the surface information, while

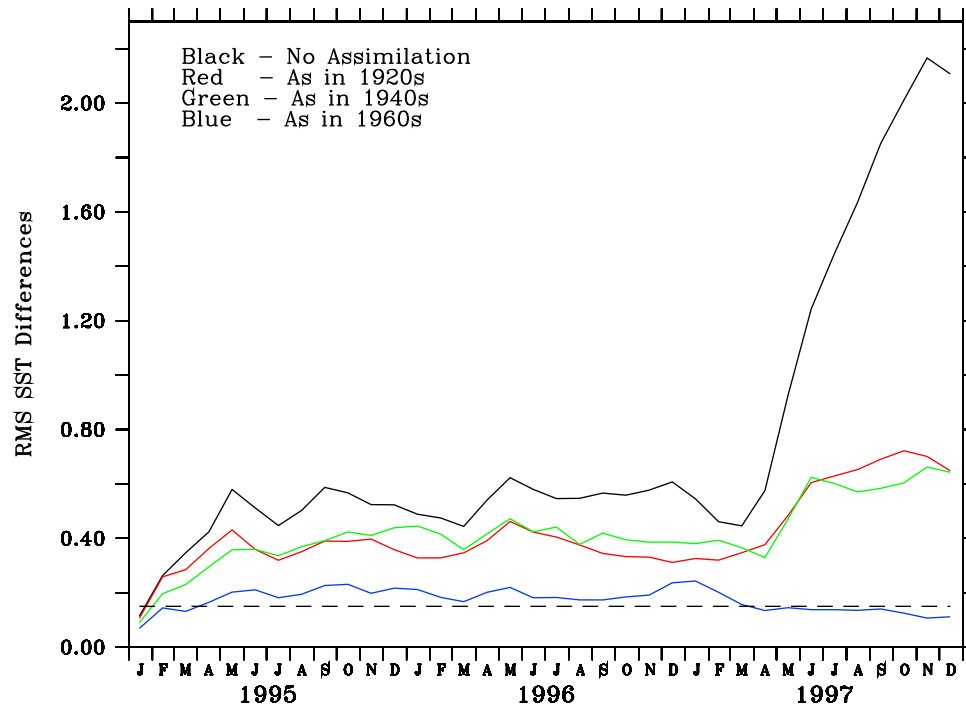


Figure 4. RMS SST difference in the tropical Pacific Ocean (120°E to 70°W and 5°S to 5°N) between the control case and an assimilation using data coverage as in the 1960s (blue line), 1940s (green line), 1920s (red line), and a run with no data assimilation (black line). The dashed line shows the expected error between two identical runs but with different initial conditions.

being important is not sufficient to reproduce the structure of these depth integrated quantities.

3. Results

3.1. Data Thinning Experiments

[24] We explore the impact of the changing observation coverage on the reanalysis by conducting a series of data thinning experiments, in which we reduce the spatial data coverage of the 1990s as though observed in the 1920s, 1940s, and 1960s. We do this by finding the latitude and longitude of observations in earlier decades and then finding a corresponding observation in the 1990s. In addition we limit the 1990s observation to the depth range of the earlier observation. The initial and surface boundary conditions are identical in all of the experiments; the only difference is the amount of data going into the assimilation. For these experiments we use climatological forcing, so that we can isolate the data as a contributing factor to interannual variability. We also conduct an experiment with no data assimilation as a comparison.

[25] The impact of varying data density in the thinned experiments is summarized in Figure 4 which shows the RMS difference in the tropical Pacific Ocean (120°E to 70°W and 5°S to 5°N) between the thinned experiments and the control run which uses all of the data from the 1990s. The no assimilation case is shown in black, the 1920s case is shown in red, the 1940s case is shown in green, and the 1960s case is shown in blue. The dashed line shows the expected error between two runs that are identical except for different initial conditions. We do not expect agreement to consistently exceed this level. The results presented in

Figure 4 show that the data present in the 1960s are sufficient to capture SST variability as well as the 1990s. There is more error in the 1920s and 1940s; however, in both cases the error is much less than for the case where no data are assimilated. Even in times of relatively sparse data coverage, the assimilation of data adds value to the reanalysis. In section 3.2 we also address the issue of model bias by comparing the assimilation run with an identical run, but without assimilation.

3.2. Niño 3.4

[26] We begin by exploring SST anomalies in the Niño 3.4 region (averaged from 170°W to 120°W and from 5°S to 5°N) associated with ENSO for the period from 1871 to 2008. To construct the time series of temperature anomaly, climatology must first be removed. For short records it is clear that this climatology should be calculated using the entire record. For longer records, in which there may be prominent trends or variability, it is less clear over which period the climatology should be calculated. Since we are interested in the low-frequency (decadal) behavior of ENSO, we attempt to remove low-frequency variations in the climatology from the time series, so that we retain only the interannual component. We do this by allowing the climatology, from which the SST anomalies are constructed, to evolve as a function of time. SST in the Niño 3.4 region is shown in Figure 5a. The actual SST is plotted in black, and a climatology based on an 11 year moving window is plotted in red. For the first and last 5 years a constant climatology is used based on the first and last 11 years, respectively. Although there are periods of time, for example, from 1890 to 1910, when the mean Niño 3.4 SST is higher than the

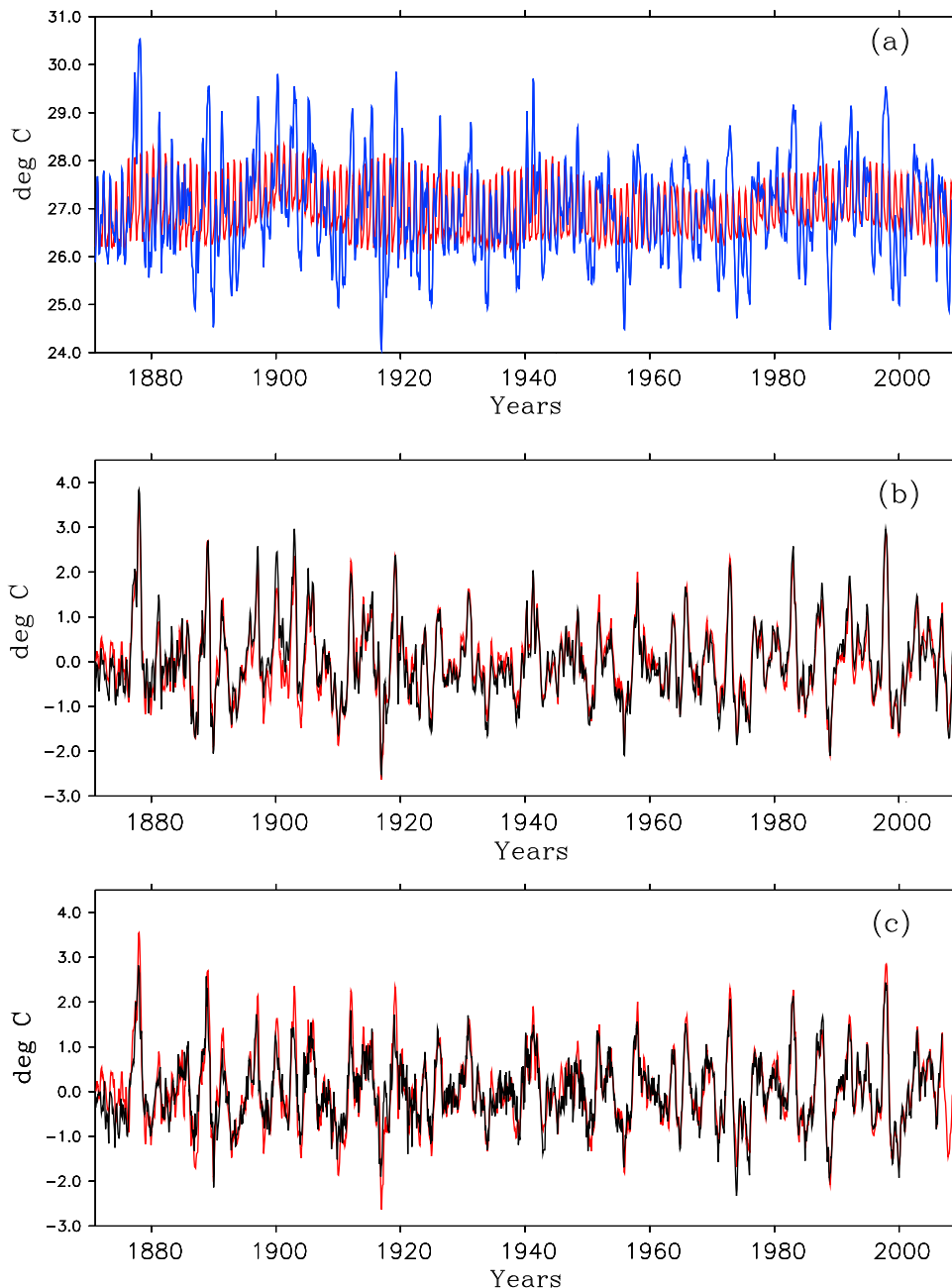


Figure 5. (a) Niño 3.4 (170°W to 120°W and 5°S to 5°N) SST from SODA 2.2.4. Superimposed in red is an 11 year running climatology. (b) Niño 3.4 SST anomaly from SODA 2.2.4 plotted with the 11 year running climatology removed (red line) and with a constant climatology based on the period 1871–2008 removed (black line). (c) Niño 3.4 SST anomaly from SODA 2.2.4 (red line) and from HadISST (black line). In both an 11 year running climatology has been removed.

long-term average the climatology is actually fairly constant across the entire record. This approach, similar to that used by *Fedorov and Philander* [2000], creates a climatology that is long enough that it does not get distorted by strong El Niño events, but is short enough to remove much of the decade-to-decade variability and trends that make it difficult to analyze interannual variability.

[27] In Figure 5b we show Niño 3.4 SST anomaly calculated with both the 11 year moving window climatology and the climatology calculated using the entire record. Using

the 11 year moving window climatology reduces the amplitude of El Niño events in the last part of the 19th century and the beginning part of the 20th century by about 0.5°C and warms El Niño events from 1919 to 1960 by about 0.25°C . The El Niño events after 1980 are largely unaffected by using the 11 year moving window climatology.

[28] The NOAA definition of El Niño years is when the Niño 3.4 SST anomaly exceeds 0.5°C for 3 consecutive months. By this measure 1877 is the strongest El Niño with an SST anomaly of 3.5°C , followed by 1997 (2.8°C).

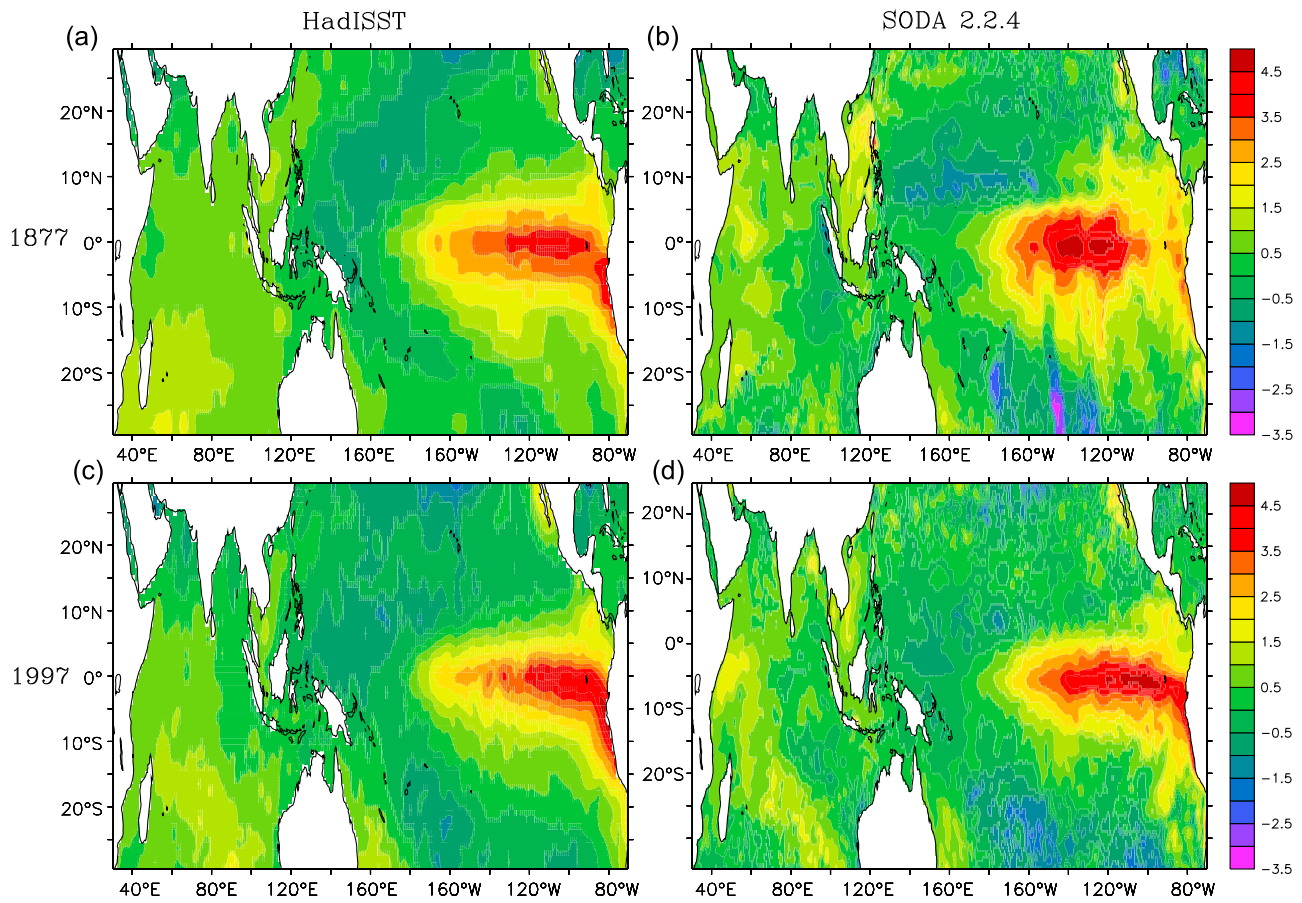


Figure 6. SST anomaly for the 1877 El Niño in (a) HadISST and (b) SODA 2.2.4 and for the 1997 El Niño in (c) HadISST and (d) SODA 2.2.4.

Although the Niño 3.4 index is a well-accepted measure of El Niño, it is fixed in space and so in many ways is not a good measure if the structure of El Niño varies.

[29] The Niño 3.4 SST anomaly from SODA 2.2.4 and from HadISST is shown in Figure 5c. The most striking aspect of the two lines is their high correlation ($r = 0.9$). In the latter half of the 20th century it is expected that the two estimates of SST should agree because the same observations are used in both analyses. But in the first half of the record there is not nearly as much data available, and it is not clear that there should be such good agreement.

[30] The number of observations that go into the Niño 3.4 SST reconstruction are limited in the first half of the 20th century. Thus, during these early years the Niño 3.4 SST reconstruction relies heavily on assumed geographic patterns together with SST observations outside of the Niño 3.4 region and thus should be considered tentative.

[31] In fact, closer inspection of Figure 5c shows that there are considerable differences between SODA 2.2.4 and HadISST in the first half of the 20th century. It is not that the two products disagree about whether there was an El Niño, but they disagree with respect to the strength and location of the El Niños.

[32] SODA 2.2.4 shows an extraordinary period of time, from 1890 to 1920, during which there were frequent powerful El Niño events, with four of these events as strong as the El Niño events in the last half of the 20th century. In

particular, the reanalysis reaffirms the strength of the 1918/1919 El Niño described by *Giese et al.* [2010] as being one of the strongest of the 20th century. Although the reanalysis and the HadISST reconstructed SST agree about the strength of some of these events, the reanalysis shows that the four strongest El Niño events during this period are 0.5° to 1°C larger in the reanalysis than in the reconstruction.

[33] The reanalysis also shows that there are strong La Niña events at the beginning of the 20th century, another feature in common with the latter part of the 20th century. In between these two periods of strong El Niño events is a lengthy period, from 1920 to 1970, during which El Niño events appear to be weaker. Interestingly, the La Niña events in the middle of the 20th century are weak as well.

[34] An inspection of the spatial patterns of SST anomaly shows that there are considerable event-to-event differences in the structure of El Niño events. The December-January-February (DJF) SST anomaly for the two largest El Niño events on record from SODA 2.2.4 and HadISST are shown in Figure 6a and 6b for the 1877/1878 El Niño and Figures 6c and 6d for the 1997/1998 El Niño. As might be expected, when there are ample data, for example, during the 1997/1998 El Niño, the two products agree quite well in terms of the location and amplitude of warming. In contrast, during the 1877/1878 El Niño for which there are only sparse observations, the location of the El Niño is quite different in the two products.

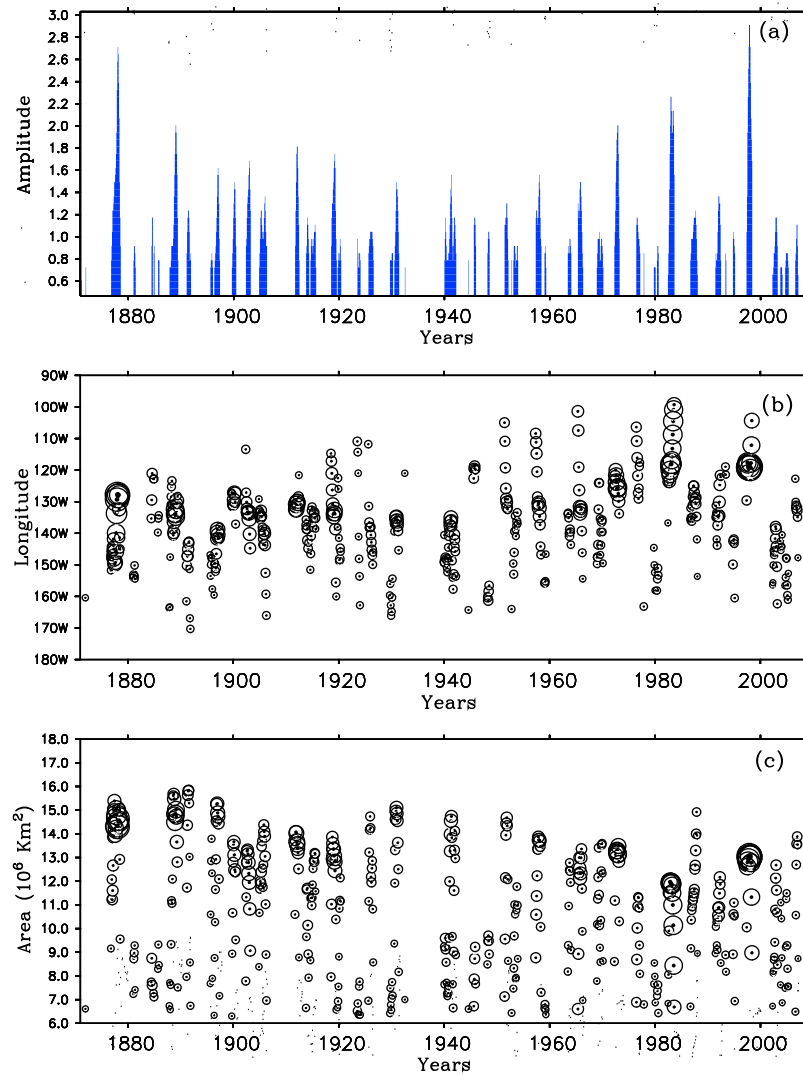


Figure 7. (a) The CHI amplitude from SODA 2.2.4 in $^{\circ}\text{C}$. (b) The CHI longitude from SODA 2.2.4. (c) The CHI area from SODA 2.2.4 in 10^6 km^2 .

[35] The HadISST El Niño of 1877/1878 shows an El Niño event that is markedly similar to the El Niño of 1997/1998 (compare Figures 6a and 6c). The two El Niños are different in the SODA reanalysis, with the largest SST anomalies in 1877/1878 displaced to the west of the coast of South America. These contrasting El Niño events highlight two issues of concern for the historical representation of El Niño. By design the HadISST reconstruction relies on SST anomaly patterns obtained in periods of dense observations to extrapolate into regions of sparse observations in earlier years.

[36] The second issue of concern is that it is apparent that Niño 3.4 SST anomaly may be an inaccurate measure of El Niño strength when the El Niño is not located in the Niño 3.4 region. For example, Figure 5c shows that the 1877/1878 El Niño is stronger than the 1997/1998 El Niño using Niño 3.4 as an indicator of El Niño strength, whereas Figures 6b and 6c suggest that the 1997/1998 El Niño is as strong, or stronger than, the 1877/1878 El Niño. In fact, some other indices such as the Trans Niño index [Trenberth and Stepaniak 2001] and El Niño Modoki

index [Ashok *et al.*, 2007] have been defined to capture the structurally variable nature of El Niño.

3.3. Center of Heat Index

[37] In an attempt to formulate an index that is more representative of spatially varying El Niño, we calculate the first moment of the SST anomaly, which we call the center of heat index (CHI). The new index is based on the location of SST anomalies greater than 0.5°C within a strip that spans the tropical Pacific (from 120°E to 70°W and from 5°S to 5°N). The index gives the temperature-weighted center (in terms of longitude) of the area over which the warm anomaly ($>0.5^{\circ}\text{C}$) exists only if this warm area is greater than or equal to the area of the Niño 3.4 region. The CHI has three components: the CHI longitude given by

$$\text{CHI longitude} = \frac{\sum \text{sst_anom} \times \text{longitude}}{\sum \text{sst_anom}} \quad (1)$$

where sst_anom is the SST anomaly $> 0.5^{\circ}\text{C}$ subject to the constraint that the total area of SST anomaly (CHI area) is

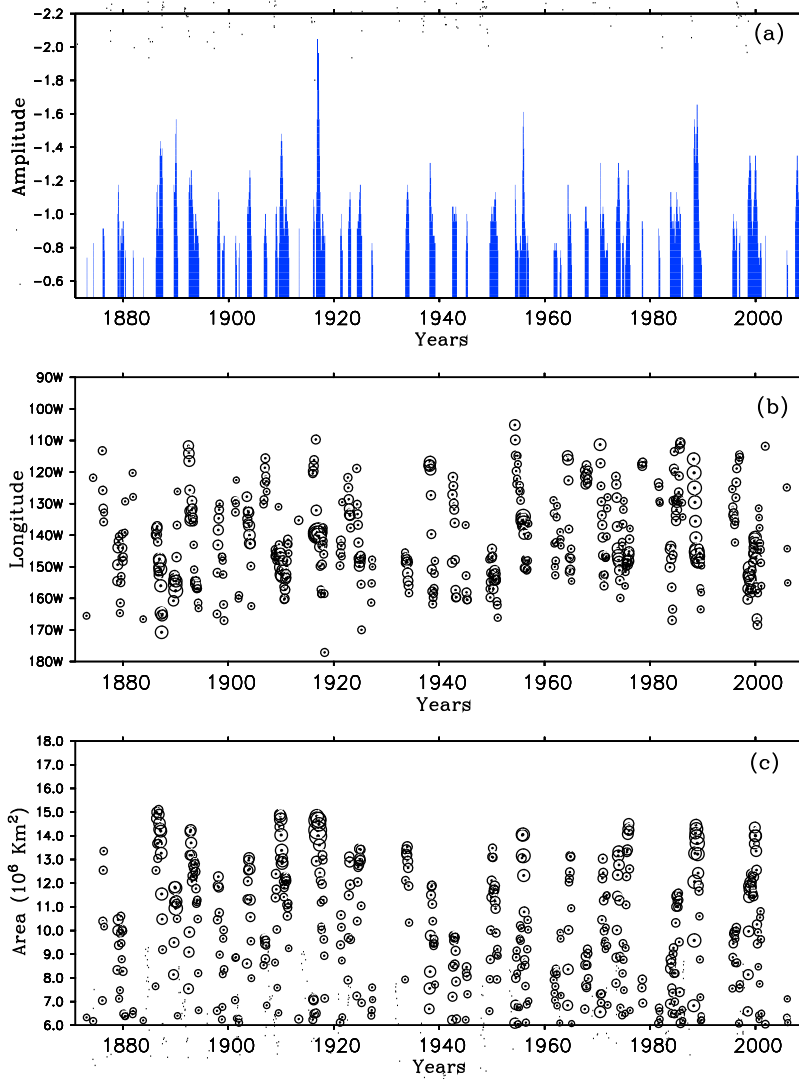


Figure 8. Same as in Figure 7 except for La Niña conditions.

greater than the area of the Niño 3.4 region, and the CHI amplitude given by

$$\text{CHI amplitude} = \frac{\sum \text{sst_anom} \times \text{area}}{\sum \text{area}} \quad (2)$$

where area is the area of temperature anomaly > 0.5°C.

[38] The CHI amplitude is plotted in Figure 7a for the period from 1871 through 2008. The CHI amplitude shows prominent decadal variability of El Niño, with strong El Niño events from the beginning of the record to about 1920 and again from about 1970 to the end of the 20th century. In between, from 1920 through the 1960s there are fewer, and weaker, El Niños. It is interesting to note that the period from 1930 to 1940 is fairly unique in the time series for a distinct lack of El Niños.

[39] The central location of the warm anomaly (CHI longitude) is shown in Figure 7b, and also shows considerable variability. In this plot the strength (CHI amplitude) of the El Niño is represented by the size of the circle centered

at the CHI longitude. El Niños are centered at longitudes from just east of the dateline to 100°W. There is a tendency for El Niño events, particularly strong events, to be farther to the east in the second half of the 20th century, but weak events in the central and western Pacific occur throughout the record. Unlike CHI strength, there is not a clear indication of a decadal signal although there is a very modest eastward trend of the CHI longitude. The area covered by anomalous warm water is shown in Figure 7c, and as for CHI longitude, the radius of the circle is scaled proportional to CHI amplitude. CHI area shows that El Niño events have a wide range of areas; however, it is clear that weak El Niños tend to cover smaller areas. There is a clear indication of a trend suggesting that in recent years strong El Niños cover less area than in the beginning of the record. For example the 1997/1998 El Niño covers much less surface area than the 1877/1878 El Niño, even though they are comparable in amplitude.

[40] The CHI indices can also be used to evaluate La Niña events by replacing the 0.5°C criteria with -0.5°C. The CHI

Table 1. List of El Niño and La Niña Years Based on CHI Amplitude^a

	DJF	JFM	FMA	MAM	AMJ	MJJ	JJA	JAS	ASO	SON	OND	NDJ
1871												
1872												
1873												
1874												
1875												
1876		-0.9	-0.9	-0.9	-0.9	-0.8				0.8	0.9	1.1
1877	1.2	1.3	1.3	1.4	1.5	1.5	1.6	1.6	1.8	2.0	2.3	2.6
1878	2.7	2.6	2.4	2.1	1.5	1.2	0.9					-1.0
1879	-1.1	-1.2	-1.0	-0.8		-0.8	-0.9	-0.9	-0.8	-0.8	-0.9	-1.0
1880	-0.9	-0.9										
1881	0.8	0.9	0.9	0.8	0.7							
1882												
1883												
1884												
1885												
1886		-0.8	-0.9	-1.1	-1.2	-1.1	-0.9	-0.9	-1.0	-1.2	-1.3	
1887	-1.4	-1.4	-1.4	-1.3	-1.4	-1.2	-0.9			0.8	0.7	
1888	0.7	0.8	0.9	0.9	0.9	1.0	1.1	1.3	1.6	1.8	2.0	
1889	2.0	1.9	1.8	1.5	1.2	0.8		-1.2	-1.1	-1.1	-1.3	-1.5
1890	-1.6	-1.3	-1.0	-0.9	-0.7							
1891		0.8	1.0	1.2	1.2	1.3	1.2	1.1	0.8	0.8	0.8	
1892					-1.1	-1.2	-1.2	-1.1	-1.2	-1.3	-1.3	
1893	-1.2	-1.1	-1.0	-1.0	-0.9	-0.8	-0.8	-0.9	-1.0	-1.0	-0.9	
1894	-0.9	-0.9	-0.9	-0.8	-0.8							
1895							0.7	0.8	0.8	0.8	0.8	
1896	0.7				0.7	0.8	0.8	0.9	1.0	1.2	1.4	1.5
1897	1.6	1.6	1.3	1.0	0.8						-0.9	-1.0
1898	-1.1	-1.1	-1.1	-1.0	-0.8					-0.8	-0.8	-0.8
1899	-0.8	-0.9	-0.9					0.7	0.8	1.0	1.2	
1900	1.3	1.5	1.5	1.4	1.2	0.9						
1901												
1902					0.9	1.0	1.2	1.3	1.4	1.4	1.6	1.7
1903	1.6	1.4	1.3			-1.1	-1.0	-1.0	-1.1	-1.2	-1.2	
1904	-1.3	-1.2	-1.1	-0.9	-0.8					0.7	0.9	
1905	1.0	1.2	1.2	1.2	1.1	1.0	1.0	1.0	1.2	1.3	1.4	
1906	1.2	1.0	0.9	0.9				-0.8	-0.9	-0.9	-1.0	
1907	-1.0	-0.9	-0.8	-0.7								
1908											-0.8	-1.0
1909	-1.1	-1.0	-0.9	-0.8		-0.7	-0.8	-1.0	-1.2	-1.4	-1.4	
1910	-1.5	-1.4	-1.4	-1.2	-1.1	-0.9	-0.9	-0.9	-1.0	-1.1	-1.1	-1.1
1911	-1.0	-1.0	-1.0	-0.9	-0.9	-0.7		0.9	1.2	1.5	1.7	
1912	1.8	1.8	1.6	1.4	1.1	0.8						
1913										0.8	0.9	1.1
1914	1.2	1.1	1.0	0.8			0.8	0.9	1.0	1.0	0.9	
1915	0.9	0.9	1.0	1.0	1.1	1.1	1.0	0.7				
1916							-1.0	-1.2	-1.6	-1.9	-2.1	
1917	-2.0	-1.7	-1.6	-1.4	-1.2	-0.9	-0.8	-0.8	-0.9	-1.0	-1.0	-1.0
1918	-0.9	-0.9	-0.9	-0.9		1.0	1.2	1.3	1.3	1.4	1.5	
1919	1.6	1.7	1.7	1.6	1.3	1.0	0.8		0.7	0.9	0.8	
1920	0.8	0.9	1.0	0.9	0.8							
1921		-0.9	-0.9	-1.0	-0.9	-0.8	-0.8					
1922								-0.9	-1.0	-1.0	-1.1	
1923	-1.2	-1.1	-0.9			1.0	0.9	0.7	0.7	0.8	0.9	
1924	0.8				-0.9	-0.9	-1.0	-1.0	-1.0	-1.1	-1.2	
1925	-1.2	-1.0	-0.9	-0.9			0.8	0.9	1.0	1.0	1.0	
1926	1.0	1.1	1.1	1.1	1.0	0.9	0.8					
1927												
1928												
1929							0.8	0.8	0.8	0.8	0.8	
1930	0.8	0.8	0.8			0.8	0.9	1.1	1.2	1.4	1.5	
1931	1.4	1.3	1.2	1.0	0.9							
1932												
1933						-0.8	-0.9	-1.0	-1.1	-1.2	-1.2	
1934	-1.1	-1.1	-1.0	-0.8								
1935												
1936												
1937												
1938	-1.1	-1.3	-1.3	-1.2	-1.0	-1.0	-1.0	-1.0	-0.9	-0.9	-0.9	

Table 1. (continued)

	DJF	JFM	FMA	MAM	AMJ	MJJ	JJA	JAS	ASO	SON	OND	NDJ	
1939	-0.9	-0.8	-0.8										
1940	0.8	1.0	1.1	1.1	0.9	0.8	0.8	0.8	0.8	0.9	0.9	1.0	
1941	1.1	1.3	1.5	1.5	1.4	1.1	0.9	0.8	0.9	1.0	1.1	1.2	
1942	1.1	1.0	0.9			-1.0	-1.0	-1.0	-1.0	-1.0	-1.0	-1.0	
1943	-1.0	-1.0	-1.0	-0.9									
1944													
1945	-0.8	-0.9	-1.0	-1.0	-0.8			1.1	1.2	1.2	1.1	0.9	
1946													
1947													
1948			0.8	1.0	1.1	1.1	1.0						
1949							-0.8	-0.8	-0.9	-1.0	-1.0	-1.0	
1950	-1.0	-0.9	-1.0	-1.0	-1.1	-1.1	-1.1	-1.1	-1.1	-0.9	-0.9	-0.9	
1951	-0.9	-0.8				1.1	1.1	1.2	1.2	1.3	1.3	1.2	
1952	1.0	0.8											
1953		0.8	0.9	0.9	0.9	0.8	0.8	0.8	0.8	0.9	0.9	0.8	
1954						-1.2	-1.1	-1.0	-0.9	-0.8	-0.8	-0.8	
1955			-0.7	-0.8	-0.9	-0.9	-0.8	-0.8	-1.0	-1.3	-1.5	-1.6	
1956	-1.4	-1.2	-1.0	-0.9	-0.9	-0.8		-0.8	-0.8	-0.9	-0.8	-0.8	
1957						1.2	1.3	1.2	1.2	1.1	1.2	1.3	1.5
1958	1.6	1.4	1.2	1.0	0.9								
1959													
1960													
1961										-0.8	-0.8	-0.8	-0.8
1962	-0.8	-0.8	-0.8	-0.8	-0.7								
1963							0.9	0.9	0.9	0.9	1.0	1.0	0.9
1964	0.8						-1.2	-1.2	-1.0	-0.9	-0.9	-1.0	-1.0
1965	-0.8	-0.7					1.3	1.3	1.2	1.3	1.4	1.5	1.4
1966	1.2	1.1	0.9	0.7									
1967								-1.0	-1.0	-1.0	-1.0	-1.0	
1968	-0.9	-0.9	-0.9	-0.9								0.7	
1969	0.9	1.0	1.0	1.0	1.0	1.0	1.0	0.8	0.8	0.9	1.0	1.0	0.9
1970	0.8	0.8						-1.3	-1.0	-0.9	-0.9	-1.0	-1.0
1971	-1.0	-1.0	-1.0	-0.9	-0.8	-0.7	-0.7	-0.8	-0.8	-0.8	-0.8	-0.8	-0.8
1972					0.9	1.1	1.2	1.5	1.7	1.9	1.9	2.0	2.0
1973	1.7	1.4	1.0					-1.0	-1.0	-1.1	-1.1	-1.2	-1.3
1974	-1.3	-1.2	-1.1	-1.0	-0.8					-0.8	-0.8	-0.9	-0.8
1975	-0.8				-0.7	-0.8	-0.9	-1.0	-1.0	-1.2	-1.3	-1.2	-1.2
1976	-1.1	-0.9	-0.7				1.1	1.2	1.2	1.1	1.1	1.0	1.0
1977	0.9	0.9											
1978													
1979													
1980													
1981													
1982							0.7	0.9	1.1	1.4	1.8	2.0	2.2
1983	2.3	2.1	1.9	2.0	2.1	2.2	2.0	1.6		-1.1	-1.2	-1.1	
1984	-1.0	-0.9	-0.9	-0.9	-0.9	-0.9	-1.0	-1.0	-0.9	-0.8	-0.9	-1.0	-1.0
1985	-1.1	-1.1	-1.0	-1.0	-1.0	-1.0	-1.0	-0.9	-1.0	-1.0	-1.0	-1.0	
1986										0.8	0.9	1.0	1.0
1987	1.0	1.0	1.0	1.1	1.2	1.2	1.2	1.2	1.2	1.2	1.1	1.0	0.8
1988	0.7			-1.4	-1.6	-1.6	-1.5	-1.3	-1.3	-1.5	-1.7	-1.7	
1989	-1.5	-1.3	-1.1	-0.9	-0.8	-0.8	-0.8	-0.8	-0.7	-0.7			
1990													
1991							0.8	0.8	0.8	0.8	0.9	1.1	1.2
1992	1.4	1.3	1.3	1.3	1.1	0.8							
1993													
1994										1.0	1.1	1.0	
1995	0.9	0.9							-0.8	-0.9	-1.0	-1.0	-0.9
1996	-0.9	-0.8	-0.8	-0.9	-1.0	-0.9							
1997						1.0	1.4	1.9	2.3	2.6	2.7	2.9	2.9
1998	2.7	2.4	2.1	1.9	1.7		-1.1	-1.2	-1.2	-1.3	-1.4	-1.4	
1999	-1.3	-1.3	-1.1	-1.0	-0.9	-0.9	-1.0	-1.0	-1.1	-1.2	-1.3	-1.4	
2000	-1.4	-1.3	-1.1	-1.1	-1.0	-0.8	-0.7	-0.7	-0.7	-0.7	-0.8	-0.8	
2001	-0.8	-0.8											
2002					0.7	0.7	0.7	0.8	0.9	0.9	1.0	1.2	1.2
2003	1.2	1.1	0.9							0.7	0.7	0.8	
2004	0.7	0.7								0.8	0.8		

Table 2. Summary of El Niño and La Niña Years in Table 1

El Niño Years	Duration		La Niña Years	Duration	
	(months)	Strength		(months)	Strength
1876/1877/1878	22	2.7	1876	5	-0.9
1881	5	0.9	1878/1879/1880	14	-1.2
1888/1889	20	2.0	1886/1887	17	-1.4
1895/1896/1897	19	1.6	1889/1890	10	-1.6
1899/1900	10	1.5	1892/1893/1894	24	-1.3
1902/1903	11	1.7	1897/1898/1899	13	-1.1
1904/1905/1906	18	1.4	1903/1904	11	-1.3
1911/1912	10	1.8	1906/1907	8	-1.0
1913/1914/1915	20	1.2	1908/1909/1910/1911	30	-1.5
1918/1919/1920	21	1.7	1916/1917/1918	21	-2.1
1923/1924	7	1.0	1921	6	-1.0
1925/1926	12	1.1	1922/1923	7	-1.2
1929/1930/1931	18	1.5	1924/1925	12	-1.2
1940/1941/1942	27	1.5	1933/1934	10	-1.2
1945	5	1.2	1938/1939	14	-1.3
1948	5	1.1	1942/1943	11	-1.0
1951/1952	9	1.3	1945	5	-1.0
1953	11	0.9	1949/1950/1951	20	-1.1
1957/1958	13	1.6	1954/1955/1956	29	-1.6
1963/1964	8	1.0	1961/1962	9	-0.8
1965/1966	12	1.5	1964/1965	10	-1.2
1968/1969/1970	15	1.0	1967/1968	9	-1.0
1972/1973	12	2.0	1970/1971	18	-1.3
1976/1977	9	1.2	1973/1974/1975	28	-1.3
1982/1983	15	2.3	1983/1984/1985	25	-1.2
1986/1987/1988	17	1.2	1988/1989	19	-1.7
1991/1992	13	1.4	1995/1996	11	-1.0
1994/1995	5	1.1	1998/1999/2000	32	-1.4
1997/1998	13	2.9	2007/2008	12	-1.4
2002/2003	12	1.2			
2003/2004	5	0.8			
2004/2005	7	0.9			
2006/2007	7	1.1			
	12.5	1.4		15.2	-1.3
		0.50			0.27

amplitude, longitude, and area for La Niña events are shown in Figures 8a–8c. Interestingly, there is considerably less variability, both in terms of a trend or decadal variability for cold events. La Niña events tend to be more uniform for all three CHI characteristics, with little distinguishable variation across the 138 year record.

[41] The El Niño and La Niña events are summarized in Tables 1 and 2. Table 1 contains a listing of the CHI amplitude for El Niño and La Niña events from 1871 through 2008. To qualify as an El Niño, the CHI amplitude must be above 0.5°C for 5 consecutive months. There is a propensity for El Niño events to peak in northern winter of year 0 (using the terminology of *Rasmusson and Carpenter* [1982]), consistent with previous descriptions of El Niño. However, the month of highest anomaly is also highly variable, with peak anomalies occurring as early as March year 0 (1905, 1953) to as late as August year 1 (1986).

[42] Table 2 presents a summary of Table 1 and highlights the individual El Niño and La Niña events. Using CHI

amplitude to measure El Niño strength the 1997/1998 event is strongest with a peak anomaly of 2.9°C, followed by the 1876/1877/1878 El Niño with a peak anomaly of 2.7°C. Other notable El Niños include the 1982/1983 El Niño (2.3°C), 1972/1973 El Niño (2.0°C), and others with less than 2°C of warming. The mean strength of El Niño is 1.4°C and has a standard deviation of 0.5°C. Interestingly, the mean of La Niña events is similar, at -1.3°C, but has a much smaller standard deviation of just 0.27°C.

[43] Using the criteria described above as a definition of El Niño results in 33 El Niños in the period from 1871 to 2008, which results in a mean interval of 4.2 years. The mean duration of an El Niño event using the CHI criteria is 12.5 months. However, the duration of El Niño events is highly variable, extending from short events of just 5 months to the long-lived event in 1940–1942 that lasted 27 months. For La Niñas there are only 29 events, giving a frequency of every 4.8 years, but the duration, at 15.2 months, is somewhat longer than for El Niños.

[44] A question that naturally arises is the extent to which these three CHI constituents are related to each other. In Figure 9a we show CHI amplitude plotted as a function of CHI longitude. Figure 9a demonstrates that weak El Niños can occur at any longitude from just east of the dateline to about 100°W. Strong El Niños, however, tend to occur in the eastern Pacific, with the strongest events occurring between 140°W and 120°W. In Figure 9b we show CHI amplitude plotted as a function of CHI Area. There is a stronger relationship between amplitude and area than for amplitude and longitude, but overall, weak El Niños can have a wide range of areas and strong El Niños tend to be larger in area than small El Niños.

[45] The locations of all values of the CHI longitude are presented as a histogram in Figure 10 for the period from 1871 to 2008. The distribution of the data is Gaussian at the 5% significance level with a p value of 0.1374 and test statistic of 0.0373 when tested against a normal distribution having the same mean and standard deviation as the sample. A Lilliefors test is performed to test the normality of the data. The Lilliefors test is similar to the Komogorov-Smirnoff test but does not require a predetermined cumulative distribution function to test the null hypothesis.

[46] The mean of CHI longitude is 139°W and has a standard deviation of 12.8°. The data have a positive skewness of 0.1123 implying that the peak is shifted toward the central Pacific away from the South American coast. The Gaussian that gives the smallest RMS difference between the CHI and the distribution is plotted as a dashed line in Figure 10. This Gaussian has a mean of 139°W and a standard deviation of 12.8°. The null hypothesis is that El Niño events have a single mean location, and that the varying longitude of El Niño can be represented as a Gaussian distribution about that mean. The Gaussian that is fitted to the histogram uses the mean of the data (CHI longitude) and a standard deviation, which is the square root of the best unbiased estimate of the variance of the data,

Notes to Table 1:

^aCHI amplitude is described in the text. To qualify as an El Niño or La Niña, there must be 5 consecutive months for which the CHI amplitude exceeds 0.5°C. DJF, December-January-February; JFM, January-February-March; FMA, February-March-April; MAM, March-April-May; AMJ, April-May-June; MJJ, May-June-July; JJA, June-July-August; JAS, July-August-September; ASO, August-September-October; SON, September-October-November; OND, October-November-December; NDJ, November-December-January.

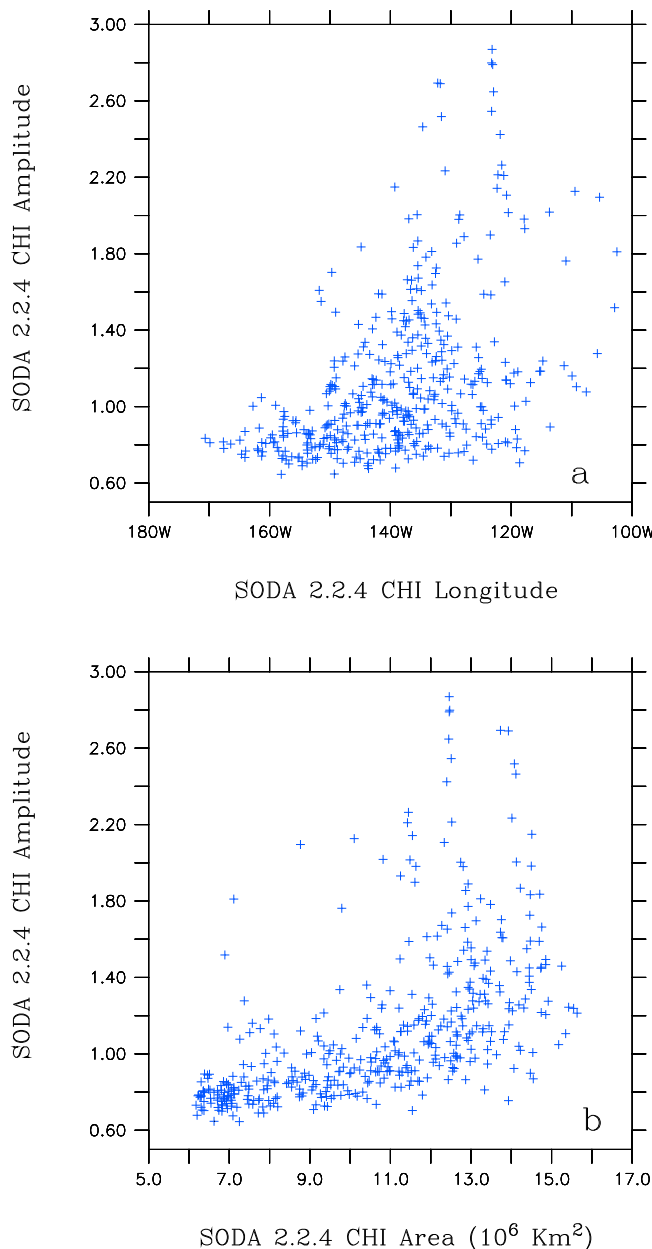


Figure 9. (a) CHI amplitude plotted as a function of CHI longitude for SODA 2.2.4. (b) CHI amplitude plotted as a function of CHI area for SODA 2.2.4.

considering the data to be a sample of a normal distribution. The fitted Gaussian confirms the uniform location of CHI longitude to be at or around a particular longitude on the equatorial Pacific. Using the Lilliefors test [Conover, 1980], the distribution in Figure 10 cannot be distinguished from the Gaussian distribution; thus, the null hypothesis cannot be rejected.

[47] We changed the threshold criteria for the area of anomalous warming from being equal to the Niño 3.4 area to half of Niño 3.4 area and we reduced the anomalous temperature criteria from 0.5°C to 0.25°C of anomaly to explore the sensitivity of the distribution to our criteria. Changing the threshold area and temperature to calculate

CHI longitude and CHI amplitude does not change the mean of the distribution of CHI longitude by more than a few degrees of longitude. In both cases the distribution cannot be distinguished from Gaussian.

3.4. Comparison With HadISST

[48] Figure 11a shows CHI longitude calculated using HadISST plotted as a function of CHI longitude calculated using SODA 2.2.4. The data are separated into two periods; data from before 1950 are plotted in red and data from after 1949 are plotted in blue. The regression for each period is shown as a line. Before 1950 the two products are largely uncorrelated and almost all of the El Niño events in HadISST occur to the east of where they occur in SODA. After 1949 the two products are much better correlated although HadISST has the center of El Niño farther east than SODA, particularly for those events that occur in the central to western Pacific in SODA. It is not surprising that the two products agree after 1949 when there is relatively good data coverage. The poor agreement before 1949 could be due to model bias in SODA 2.2.4 or it could be due to errors in the HadISST data set, or it could be a combination of both.

[49] One way to explore the possibility of bias in the model is to compare the assimilation with the simulation (SODA 2.2.0). The CHI longitude data for SODA 2.2.0 are plotted as a function of CHI longitude from SODA 2.2.4 in Figure 11b. In this case, the data from before 1950 show that the two products are very highly correlated, which is expected because when the data are sparse the assimilation has little impact on the model. In the period when there are more data the two products are still highly correlated, but the simulation shows a tendency for the warm events to be about 5° to the west of the west of the warming in the assimilation. If there was significant model bias in SODA 2.2.4, we would expect poor agreement after 1949.

[50] A similar analysis, but for CHI amplitude, is presented in Figures 12a and 12b. As for CHI longitude, when there is good data coverage, after 1949, the SODA 2.2.4 and HadISST (Figure 12a) products agree very well in terms of the strength of El Niño events. Before 1950, HadISST has weaker El Niños, which is particularly noticeable for strong events. It is interesting that before 1949, SODA and HadISST agree well about the amplitude of El Niño, but disagree about their position. The comparison between the simulation and the assimilation (Figure 12b) shows fairly good agreement both before 1950 and after 1949, which means that model bias in SODA does not significantly impact the reproduction of the strength of El Niño.

4. Summary and Conclusions

[51] We present results from a new ocean reanalysis that covers the period from 1871 to 2008 to explore the changing nature of El Niño. The new reanalysis (SODA 2.2.4) is similar to previous SODA reanalyses, except that it uses the 20CRv2 surface boundary conditions for momentum fluxes and for the variables used in the bulk formulae for heat and freshwater fluxes and does not use satellite observations. As in other SODA reanalyses we use all available hydrographic temperature and salinity observations from WOD09 [Boyer *et al.*, 2009] and SST observations from ICOADS 2.5. Since

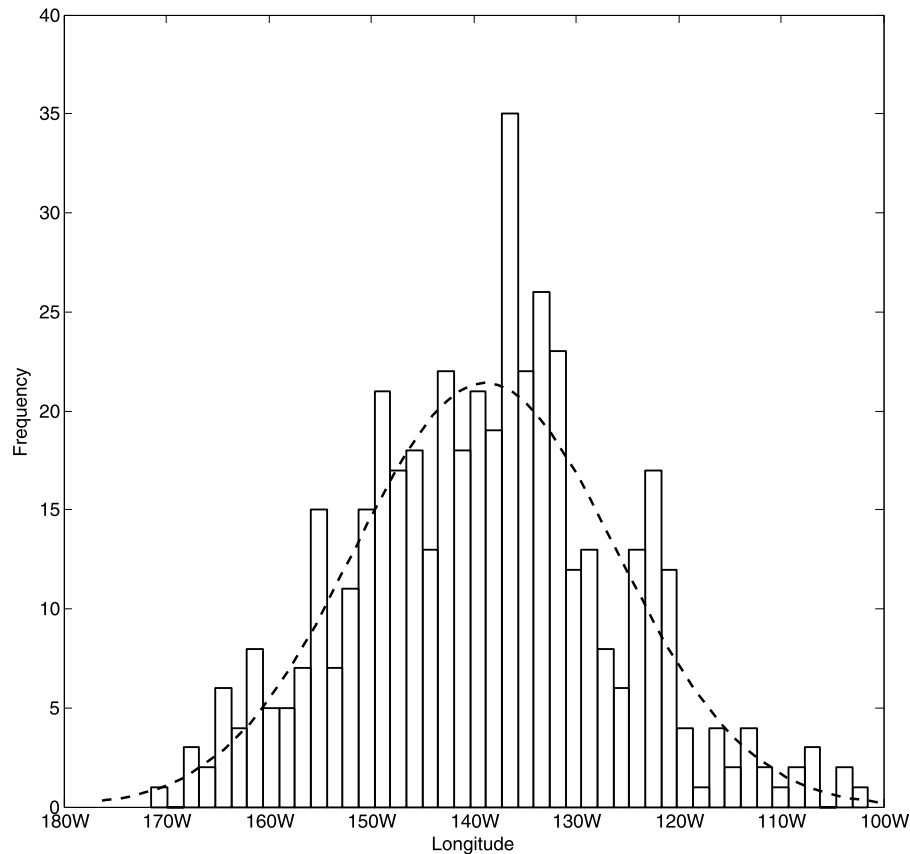


Figure 10. Histogram of CHI longitude (see Figure 7b). A Gaussian curve with the same mean and standard deviation as the CHI longitude is shown as dashed curve.

we use the standard level data from WOD09, we include the *Levitus et al.* [2009] corrections for XBT and MBT bias.

[52] Using Niño 3.4 SST anomaly as an indicator of El Niño, we show that the timing of El Niño in the reanalysis is very similar to the timing of El Niño in the HadISST reconstruction. However, the amplitude of El Niño is larger in the reanalysis. One reason for the discrepancy in amplitude between the two products is that the HadISST reconstruction relies on empirical orthogonal functions (EOFs) that are based on data from the last half of the 20th century, when there were ample observations. The record of El Niño from the reanalysis shows that many of the El Niño events from the first half of the 20th century occurred farther to the west than events in the second half of the 20th century, in a region for which there are few observations. Using the near-coastal observations and projecting onto the El Niño structure from the latter part of the 20th century likely underestimates the amplitude of El Niño events in HadISST.

[53] Since using a fixed region measure of El Niño, such as the Niño 3.4 SST anomaly, is clearly unsatisfactory for capturing the differences between El Niño events that occur at different longitudes, we develop a new index to represent El Niño. The new index, CHI, is based on the first moment of the temperature anomaly. The CHI index has three related metrics; it returns the weighted center of heat anomaly, the amplitude of the heat anomaly, and the area over which the temperature anomaly exists. Using the CHI amplitude shows that El Niño has prominent decadal variability, with large

El Niños during the last part of the 19th century and during the beginning and end of the 20th century. Relatively weak El Niños characterize the middle of the 20th century, from about 1920 to 1970. Interestingly, La Niña does not appear to undergo these decadal changes in amplitude, with relatively little change in amplitude over the 140 year period.

[54] There is also considerable variability in the location of El Niño events, with warming occurring from the central to the eastern Pacific Ocean. The location of El Niño does not appear to have the same low-frequency modulation as for the amplitude of El Niño, with a distribution of central and eastern El Niño events throughout the record. In an attempt to quantify the distribution of the location of El Niño events, we compare the distribution with a Gaussian distribution centered near 140W. The null hypothesis, that the distribution of the location of El Niño is randomly distributed about a mean value cannot be rejected.

[55] *Yeh et al.* [2009] extend the discussion of El Niño types to argue that frequency of east Pacific and central Pacific El Niño has changed in response to global warming. However, the *Yeh et al.* [2009] study relies in part on HadISST reconstructed SST. Because reconstructions rely on EOF patterns of El Niño determined in periods of time for which there are abundant observations (mostly since the late 1950s), the inferred SST patterns in the first half of the 20th century have the east Pacific El Niño embedded into the reconstructed SST. In a study of the 1918/1919 El Niño, *Giese et al.* [2010] conclude that the 1918 El Niño was

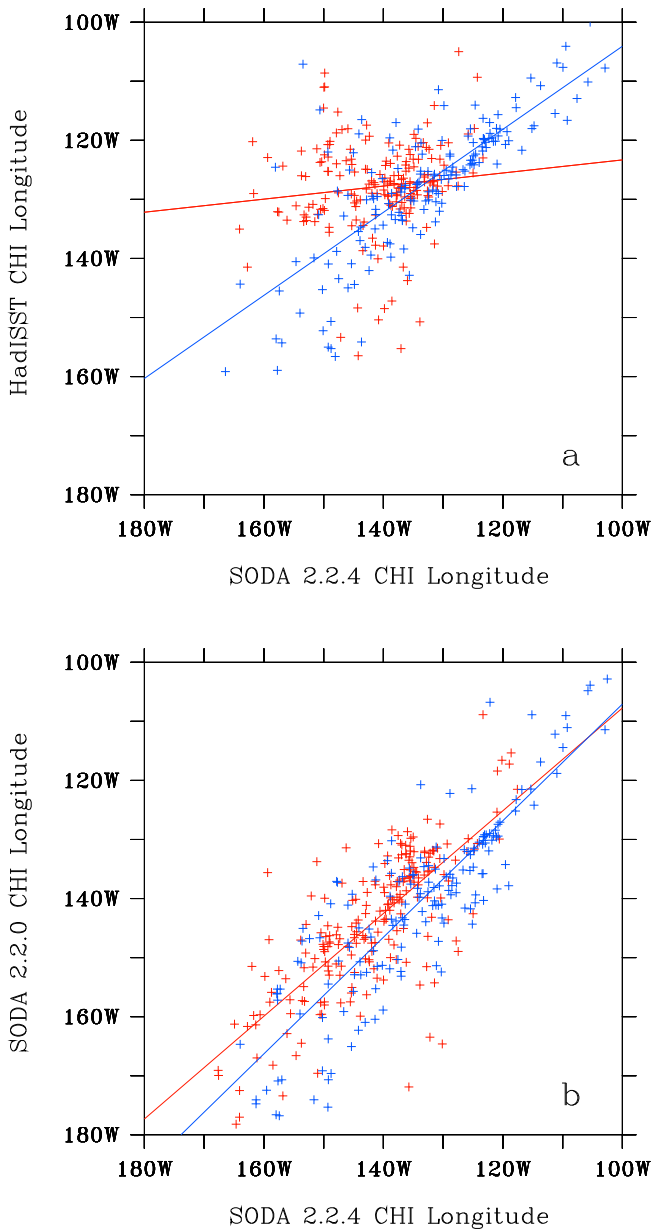


Figure 11. (a) CHI longitude from HadISST (y axis) plotted as a function of CHI longitude from SODA 2.2.4 (x axis). Values from 1871 through 1949 are shown in red, and values from 1950 through 2008 are shown in blue. The least squares regression for both periods of time are shown as a solid line. (b) CHI longitude from SODA 2.2.0 (y axis) plotted as a function of CHI longitude from SODA 2.2.4.

considerably different than that represented in the HadISST data set. In contrast with the El Niño as represented by HadISST which shows a modest east Pacific warming, the Giese *et al.* [2010] model results show a strong warming that is separated from the coast of South America.

[56] Comparing the CHI amplitude with CHI longitude shows that weak El Niño events can occur at a broad range of longitudes, but large El Niño events tend to occur in the eastern Pacific. Likewise, large El Niño events tend to have a larger area, a not entirely unexpected result.

[57] Although the SODA reanalysis shows that there is prominent decadal variability in El Niño, we have not explained the cause of the decadal changes. *Philander and Fedorov* [2003] show that El Niño is a weakly damped mode of a coupled ocean-atmosphere oscillation sustained by random disturbances such as westerly wind bursts. The properties of the oscillation depend on the background state, either as in a delayed oscillator mode [*Schopf and Suarez*, 1988; *Battisti and Hirst*, 1989] or a local mode (similar to the slow sea surface temperature mode of *Neelin* [1991])

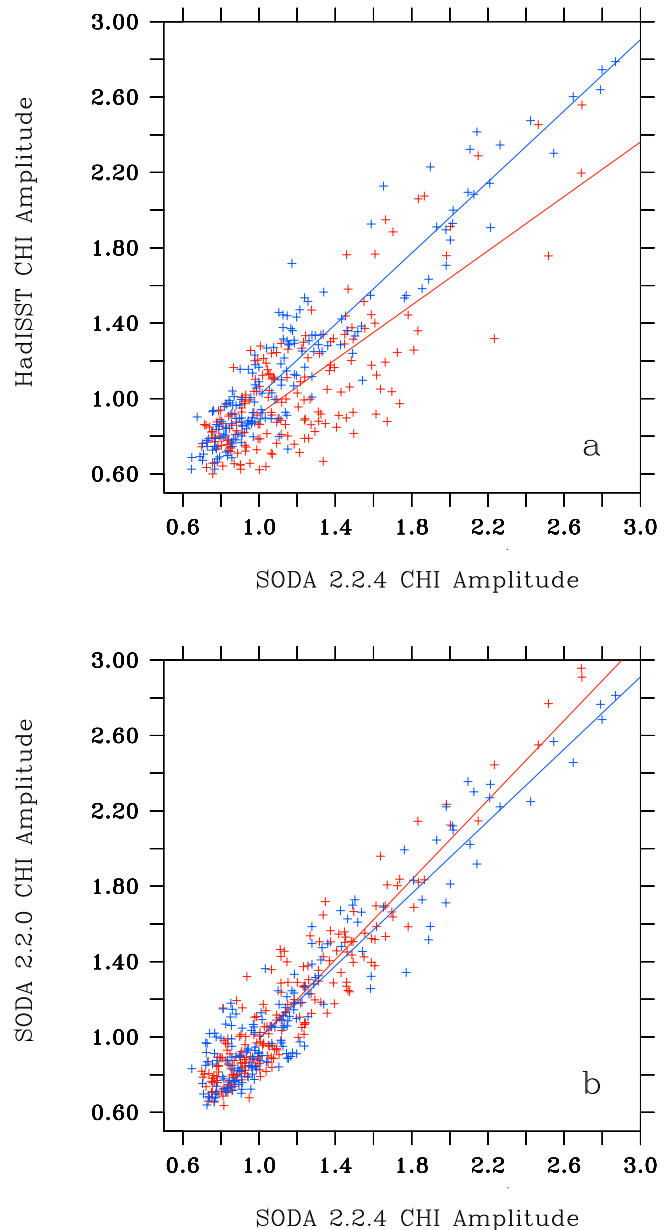


Figure 12. (a) CHI amplitude from HadISST (y axis) plotted as a function of CHI amplitude from SODA 2.2.4 (x axis). Values from 1871 through 1949 are shown in red, and values from 1950 through 2008 are shown in blue. The least squares regression for both periods of time are shown as a solid line. (b) CHI amplitude from SODA 2.2.0 (y axis) plotted as a function of CHI amplitude from SODA 2.2.4.

both of which depend on the background strength of winds and the depth and gradient of the thermocline. According to *Philander and Fedorov* [2003] it is these two modes that undergo decadal modulation giving rise to decadal variability in El Niño. We hope that ongoing studies using SODA and other ocean reanalyses will shed light on this important topic.

[58] **Acknowledgments.** Financial support for this research has been provided to B.S.G. and S.R. by NOAA (grant NA06OAR4310146 and grant NA06OAR4310146) and NSF (grant OCE-0752057).

References

- AchutaRao, K. M., B. D. Santer, P. J. Gleckler, K. E. Taylor, D. W. Pierce, T. P. Barnett, and T. M. L. Wigley (2006), Variability of ocean heat uptake: Reconciling observations and models, *J. Geophys. Res.*, *111*, C05019, doi:10.1029/2005JC003136.
- An, S.-I., and B. Wang (2000), Interdecadal change of the structure of the ENSO mode and its impact on the ENSO frequency, *J. Clim.*, *13*, 2044–2055, doi:10.1175/1520-0442(2000)013<2044:ICOTSO>2.0.CO;2.
- Arbic, B. K., and W. B. Owens (2001), Climatic warming of Atlantic intermediate waters, *J. Clim.*, *14*, 4091–4108, doi:10.1175/1520-0442(2001)014<4091:CWOAIW>2.0.CO;2.
- Ashok, K., S. K. Behera, S. A. Rao, H. Weng, and T. Yamagata (2007), El Niño Modoki and its possible teleconnection, *J. Geophys. Res.*, *112*, C11007, doi:10.1029/2006JC003798.
- Battisti, D. S., and A. C. Hirst (1989), Interannual variability in a tropical atmosphere-ocean model: Influence of the basic state, ocean geometry and nonlinearity, *J. Atmos. Sci.*, *46*(12), 1687–1712, doi:10.1175/1520-0469(1989)046<1687:IVATA>2.0.CO;2.
- Bloom, S. C., L. L. Takacs, A. M. da Silva, and D. Ledvina (1996), Data assimilation using incremental analysis updates, *Mon. Weather Rev.*, *124*, 1256–1271, doi:10.1175/1520-0493(1996)124<1256:DAUIAU>2.0.CO;2.
- Boyer, T. P., et al. (2009), *World Ocean Database 2009, NOAA Atlas NESDIS*, vol. 66, edited by S. Levitus, 216 pp., DVDs, U.S. Govt. Print. Off., Washington, D. C.
- Cane, M. A. (2005), The evolution of El Niño, past and future, *Earth Planet. Sci. Lett.*, *230*, 227–240, doi:10.1016/j.epsl.2004.12.003.
- Cane, M. A., and S. E. Zebiak (1985), A theory for El Niño and the southern oscillation, *Science*, *228*(4703), 1085–1087, doi:10.1126/science.228.4703.1085.
- Capotondi, A., M. A. Alexander, C. Deser, and M. J. McPhaden (2005), Anatomy and decadal evolution of the Pacific sub-tropical cells (STCs), *J. Clim.*, *18*, 3739–3758, doi:10.1175/JCLI3496.1.
- Carton, J. A., and B. S. Giese (2008), A reanalysis of ocean climate using simple ocean data assimilation (SODA), *Mon. Weather Rev.*, *136*, 2999–3017, doi:10.1175/2007MWR1978.1.
- Carton, J. A., G. Chepurin, X. Cao, and B. S. Giese (2000a), A simple ocean data assimilation analysis of the global upper ocean 1950–1995, part 1: Methodology, *J. Phys. Oceanogr.*, *30*, 294–309, doi:10.1175/1520-0485(2000)030<0294:ASODAA>2.0.CO;2.
- Carton, J. A., G. Chepurin, and X. Cao (2000b), A simple ocean data assimilation analysis of the global upper ocean 1950–1995, part 2: Results, *J. Phys. Oceanogr.*, *30*, 311–326, doi:10.1175/1520-0485(2000)030<0311:ASODAA>2.0.CO;2.
- Carton, J. A., S. A. Grodsky, and H. Liu (2008), Variability of the oceanic mixed layer 1960–2004, *J. Clim.*, *21*, 1029–1047, doi:10.1175/2007JCLI1798.1.
- Collins, M., et al. (2010), The impact of global warming on the tropical Pacific Ocean and El Niño, *Nat. Geosci.*, *3*, 391–397, doi:10.1038/ngeo868.
- Compo, G. P., J. S. Whitaker, and P. D. Sardeshmukh (2006), Feasibility of a 100-year reanalysis using only surface pressure data, *Bull. Am. Meteorol. Soc.*, *87*, 175–190, doi:10.1175/BAMS-87-2-175.
- Compo, G. P., J. S. Whitaker, and P. D. Sardeshmukh (2008), The 20th century reanalysis project, paper presented at Third WCRP International Conference on Reanalysis, Univ. of Tokyo, Tokyo, 28 Jan. to 1 Feb. (Available at http://wcrp.ipsl.jussieu.fr/Workshops/Reanalysis2008/Documents/V5-511_ea.pdf)
- Conover, W. J. (1980), *Practical Nonparametric Statistics*, 2nd ed., John Wiley, New York.
- Defant, A. (1981), *The Troposphere. Stratification and Circulation of the Atlantic Ocean, Scientific Results of the German Atlantic Expedition of the Research Vessel "Meteor" 1925–27*, vol. VI, Part I, edited by W. J. Emery, Amerind, New Delhi.
- Fedorov, A. V., and S. G. Philander (2000), Is El Niño changing?, *Science*, *288*, 1997–2002, doi:10.1126/science.288.5473.1997.
- Fedorov, A. V., C. M. Brierley, and K. Emanuel (2010), Tropical cyclones and permanent El Niño in the early Pliocene epoch, *Nature*, *463*, 1066–1070, doi:10.1038/nature08831.
- Giese, B. S., G. P. Compo, N. C. Slowey, P. D. Sardeshmukh, J. A. Carton, S. Ray, and J. S. Whittaker (2010), The 1918/19 El Niño, *Bull. Am. Meteorol. Soc.*, *91*, 177–183, doi:10.1175/2009BAMS2903.1.
- Giese, B. S., G. A. Chepurin, J. A. Carton, T. P. Boyer, and H. F. Seidel (2011), Impact of bathythermograph temperature bias models on an ocean reanalysis, *J. Clim.*, *24*, 84–93, doi:10.1175/2010JCLI3534.1.
- Goddard, L., and S. G. Philander (2000), The energetics of El Niño and La Niña, *J. Clim.*, *13*, 1496–1516, doi:10.1175/1520-0442(2000)013<1496:TEOENO>2.0.CO;2.
- Gu, D., and S. G. H. Philander (1995), Secular changes of annual and interannual variability in the tropics during the past century, *J. Clim.*, *8*, 864–876, doi:10.1175/1520-0442(1995)008<0864:SCOAAI>2.0.CO;2.
- Hanawa, K., P. Rual, R. Bailey, A. Sy, and M. Szabados (1995), A new depth-time equation for Sippican or TSK T-7, T-6 and T-4 expendable bathythermographs (XBT), *Deep Sea Res., Part I*, *42*, 1423–1451, doi:10.1016/0967-0637(95)97154-Z.
- Jones, P. W. (1999), First- and second-order conservative remapping schemes for grids in spherical coordinates, *Mon. Weather Rev.*, *127*, 2204–2210, doi:10.1175/1520-0493(1999)127<2204:FASOCR>2.0.CO;2.
- Kalnay, E., et al. (1996), The NCEP/NCAR 40-Year Reanalysis Project, *Bull. Am. Meteorol. Soc.*, *77*, 437–471, doi:10.1175/1520-0477(1996)077<0437:TNYRP>2.0.CO;2.
- Kao, H. Y., and J. Y. Yu (2009), Contrasting eastern-Pacific and central-Pacific types of ENSO, *J. Clim.*, *22*, 615–632, doi:10.1175/2008JCLI2309.1.
- Kaplan, A., M. Cane, Y. Kushnir, A. Clement, M. Blumenthal, and B. Rajagopalan (1998), Analyses of global sea surface temperature 1856–1991, *J. Geophys. Res.*, *103*(C9), 18,567–18,589, doi:10.1029/97JC01736.
- Kim, H.-M., P. J. Webster, and J. A. Curry (2009), Impact of shifting patterns of Pacific Ocean warming on North Atlantic tropical cyclones, *Science*, *325*(5936), 77–80, doi:10.1126/science.1174062.
- Kleeman, R., J. P. McCreary Jr., and B. A. Klinger (1999), A mechanism for generating ENSO decadal variability, *Geophys. Res. Lett.*, *26*(12), 1743–1746, doi:10.1029/1999GL900352.
- Kug, J.-S., F. F. Jin, and S.-I. An (2009), Two types of El Niño events: Cold tongue El Niño and warm pool El Niño, *J. Clim.*, *22*, 1499–1515, doi:10.1175/2008JCLI2624.1.
- Kumar, K. K., B. Rajagopalan, M. Hoerling, G. Bates, and M. Cane (2006), Unraveling the mystery of Indian monsoon failure during El Niño, *Science*, *314*, 115–119, doi:10.1126/science.1131152.
- Larkin, N. K., and D. E. Harrison (2005), On the definition of El Niño and associated seasonal average U.S. weather anomalies, *Geophys. Res. Lett.*, *32*, L13705, doi:10.1029/2005GL022738.
- Lee, T., and M. J. McPhaden (2010), Increasing intensity of El Niño in the central-equatorial Pacific, *Geophys. Res. Lett.*, *37*, L14603, doi:10.1029/2010GL044007.
- Levitus, S., J. I. Antonov, T. P. Boyer, R. A. Locarnini, H. E. Garcia, and A. V. Mishonov (2009), Global ocean heat content 1955–2008 in light of recently revealed instrumentation problems, *Geophys. Res. Lett.*, *36*, L07608, doi:10.1029/2008GL037155.
- Meinen, C. S., and M. J. McPhaden (2000), Observations of warm water volume changes in the equatorial Pacific and their relationship to El Niño and La Niña, *J. Clim.*, *13*, 3551–3559, doi:10.1175/1520-0442(2000)013<3551:OOWWVC>2.0.CO;2.
- Mitchell, T. P., and J. P. Wallace (1996), ENSO seasonality: 1950–78 versus 1979–92, *J. Clim.*, *9*, 3149–3161, doi:10.1175/1520-0442(1996)009<3149:ESV>2.0.CO;2.
- Neelin, J. D. (1991), The slow sea surface temperature mode and the fast-wave limit: Analytic theory for tropical interannual oscillations and experiments in a hybrid coupled model, *J. Atmos. Sci.*, *48*(4), 584–606, doi:10.1175/1520-0469(1991)048<0584:TSSSTM>2.0.CO;2.
- Nonaka, M., S.-P. Xie, and J. P. McCreary (2002), Decadal variations in the subtropical cells and equatorial Pacific SST, *Geophys. Res. Lett.*, *29*(7), 1116, doi:10.1029/2001GL013717.
- Østerhus, S., and T. Gammelsrød (1999), The abyss of the Nordic Seas is warming, *J. Clim.*, *12*, 3297–3304, doi:10.1175/1520-0442(1999)012<3297:TAOTNS>2.0.CO;2.
- Philander, S. G., and A. Fedorov (2003), Is El Niño sporadic or cyclic?, *Annu. Rev. Earth Planet. Sci.*, *31*, 579–594, doi:10.1146/annurev.earth.31.100901.141255.

- Pielke, R. A., Jr., and C. N. Landsea (1999), La Niña, El Niño, and Atlantic hurricane damages in the United States, *Bull. Am. Meteorol. Soc.*, *80*(10), 2027–2034, doi:10.1175/1520-0477(1999)080<2027:LNAENO>2.0.CO;2.
- Pohlmann, H., and R. J. Greatbatch (2006), Discontinuities in the late 1960's in different atmospheric data products, *Geophys. Res. Lett.*, *33*, L22803, doi:10.1029/2006GL027644.
- Power, S. B., and I. N. Smith (2007), Weakening of the Walker Circulation and apparent dominance of El Niño both reach record levels, but has ENSO really changed?, *Geophys. Res. Lett.*, *34*, L18702, doi:10.1029/2007GL030854.
- Power, S., T. Casey, C. Folland, A. Colman, and V. Mehta (1999), Interdecadal modulation of the impact of ENSO on Australia, *Clim. Dyn.*, *15*, 319–324, doi:10.1007/s003820050284.
- Rasmusson, E. M., and T. H. Carpenter (1982), Variations in tropical sea surface temperature and surface wind fields associated with the Southern Oscillation/El Niño, *Mon. Weather Rev.*, *110*, 354–384, doi:10.1175/1520-0493(1982)110<0354:VITSST>2.0.CO;2.
- Rasmusson, E. M., and T. H. Carpenter (1983), The relationship between eastern equatorial Pacific sea surface temperatures and rainfall over India and Sri Lanka, *Mon. Weather Rev.*, *111*, 517–528, doi:10.1175/1520-0493(1983)111<0517:TRBEEP>2.0.CO;2.
- Rayner, N. A., D. E. Parker, E. B. Horton, C. K. Folland, L. V. Alexander, D. P. Rowell, E. C. Kent, and A. Kaplan (2003), Global analyses of sea surface temperature, sea ice, and night marine air temperature since the late nineteenth century, *J. Geophys. Res.*, *108*(D14), 4407, doi:10.1029/2002JD002670.
- Ropelewski, C. F., and M. S. Halpert (1986), North American precipitation and temperature patterns associated with the El Niño/Southern Oscillation (ENSO), *Mon. Weather Rev.*, *114*, 2352–2362, doi:10.1175/1520-0493(1986)114<2352:NAPATP>2.0.CO;2.
- Ropelewski, C. F., and M. S. Halpert (1987), Global and regional scale precipitation patterns associated with the El Niño/Southern Oscillation, *Mon. Weather Rev.*, *115*, 1606–1626, doi:10.1175/1520-0493(1987)115<1606:GARSPP>2.0.CO;2.
- Schneider, E. K., B. Huang, and J. Shukla (1995), Ocean wave dynamics and El Niño, *J. Clim.*, *8*, 2415–2439, doi:10.1175/1520-0442(1995)008<2415:OWDAEN>2.0.CO;2.
- Schopf, P. S., and M. J. Suarez (1988), Vacillations in a coupled ocean-atmosphere model, *J. Atmos. Sci.*, *45*, 549–568, doi:10.1175/1520-0469(1988)045<0549:VIACOM>2.0.CO;2.
- Smith, R. D., J. K. Dukowicz, and R. C. Malone (1992), Parallel ocean general circulation modeling, *Physica D*, *60*, 38–61, doi:10.1016/0167-2789(92)90225-C.
- Sturaro, G. (2003), A closer look at the climatological discontinuities present in the NCEP/NCAR reanalysis temperature due to the introduction of satellite data, *Clim. Dyn.*, *21*, 309–316, doi:10.1007/s00382-003-0334-4.
- Timmermann, A., J. Oberhuber, A. Bacher, M. Esch, M. Latif, and E. Roeckner (1999), Increased El Niño frequency in a climate model forced by future greenhouse warming, *Nature*, *398*, 694–697, doi:10.1038/19505.
- Timmermann, A., S.-I. An, U. Krebs, and H. Goosse (2005), ENSO suppression due to weakening of the North Atlantic Thermohaline Circulation, *J. Clim.*, *18*, 3122–3139, doi:10.1175/JCLI3495.1.
- Trenberth, K. E., and T. J. Hoar (1996), The 1990–1995 El Niño–Southern Oscillation event: Longest on record, *Geophys. Res. Lett.*, *23*(1), 57–60, doi:10.1029/95GL03602.
- Trenberth, K. E., and T. J. Hoar (1997), El Niño and climate change, *Geophys. Res. Lett.*, *24*(23), 3057–3060, doi:10.1029/97GL03092.
- Trenberth, K. E., and D. P. Stepaniak (2001), Indices of El Niño evolution, *J. Clim.*, *14*, 1697–1701, doi:10.1175/1520-0442(2001)014<1697:LIOENO>2.0.CO;2.
- Uppala, S. M., et al. (2005), The ERA-40 reanalysis, *Q. J. R. Meteorol. Soc.*, *131*, 2961–3012, doi:10.1256/qj.04.176.
- Vecchi, G. A., and A. T. Wittenberg (2010), El Niño and our future climate: Where do we stand?, *Wiley Interdiscip. Rev. Clim. Change*, *1*, 260–270, doi:10.1002/wcc.33.
- Vecchi, G. A., B. J. Soden, A. T. Wittenberg, I. M. Held, A. Leetma, and M. J. Harrison (2006), Weakening of tropical Pacific atmospheric circulation due to anthropogenic forcing, *Nature*, *441*, 73–76, doi:10.1038/nature04744.
- Vecchi, G. A., A. Clement, and B. J. Soden (2008), Examining the tropical Pacific's response to global warming, *Eos Trans. AGU*, *89*, 81, doi:10.1029/2008EO090002.
- Wang, B. (1995), Interdecadal changes in El Niño onset in the last four decades, *J. Clim.*, *8*, 267–285, doi:10.1175/1520-0442(1995)008<0267:ICIENO>2.0.CO;2.
- Wang, B., and S. An (2001), Why the properties of El Niño changed during the late 1970s, *Geophys. Res. Lett.*, *28*(19), 3709–3712, doi:10.1029/2001GL012862.
- Whitaker, J. S., and T. M. Hamill (2002), Ensemble data assimilation without perturbed observations, *Mon. Weather Rev.*, *130*, 1913–1924, doi:10.1175/1520-0493(2002)130<1913:EDAWPO>2.0.CO;2.
- Whitaker, J. S., G. P. Compo, X. Wei, and T. M. Hamill (2004), Reanalysis without radiosondes using ensemble data assimilation, *Mon. Weather Rev.*, *132*, 1190–1200, doi:10.1175/1520-0493(2004)132<1190:RWRUED>2.0.CO;2.
- Woodruff, S. D., et al. (2011), ICOADS Release 2.5: Extensions and enhancements to the surface marine meteorological archive, *Int. J. Climatol.*, doi:10.1002/joc.2103, in press.
- Yang, H., and Q. Zhang (2008), Anatomizing the ocean's role in ENSO changes under global warming, *J. Clim.*, *21*, 6539–6555, doi:10.1175/2008JCLI2324.1.
- Ye, Z., and W. W. Hsieh (2008), Changes in ENSO and associated overturning circulations from enhanced greenhouse gases by the end of the twentieth century, *J. Clim.*, *21*, 5745–5763, doi:10.1175/2008JCLI1580.1.
- Yeh, S.-W., J.-S. Kug, B. Dewitte, M.-H. Kwon, B. P. Kirtman, and F. F. Jin (2009), El Niño in a changing climate, *Nature*, *461*, 511–514, doi:10.1038/nature08316.
- Zhang, Q., Y. Guan, and H. Yang (2008), ENSO amplitude change in observation and coupled models, *Adv. Atmos. Sci.*, *25*, 361–366, doi:10.1007/s00376-008-0361-5.

B. S. Giese and S. Ray, Department of Oceanography, Texas A&M University, College Station, TX 77843-3146, USA. (b-giese@tamu.edu)